Stability Analysis of Detailed Power System Models

by

William D. Rosehart

A thesis
presented to the University of Waterloo
in fulfillment of the
thesis requirement for the degree of
Master of Applied Science
in
Electrical Engineering

Waterloo, Ontario, 1997

©William D. Rosehart, 1997

I hereby declare that I am the sole author of this thesis.
I authorize the University of Waterloo to lend this thesis to other institutions or individuals for the purpose of scholarly research.

William D. Roschart

I authorize the University of Waterloo to reproduce this thesis by photocopying or other means, in total or in part, at the request of other institutions or individuals for the purpose of scholarly research.

William D. Roschart

The University of Waterloo requires the signatures of all persons using or photocopying this thesis. Please sign below, and give address and date.

Acknowledgments

I wish to thank Professor Claudio A. Cañizares for his guidance and support.

I also wish to thank my colleagues and friends for many interesting and entertaining discussions.

The support and encouragement of my family has been invaluable and has been greatly appreciated.

Abstract

This thesis presents a bifurcation analysis of several power system models. Different modeling levels with their respective differential-algebraic equations are studied, to determine the minimum dynamic model that adequately captures all required phenomena encountered in bifurcation studies.

A methodology for eliminating algebraic equations from the system model is proposed. The proposed model is tested on a sample system. The steady state solution of the proposed model is compared to traditional load flow solution techniques. The transient response of the proposed model is also compared to a traditional transient stability model by simulating a three phase fault.

Contents

List of Tables

List of Figures

Chapter 1

Introduction

Voltage stability problems in power systems may occur for a variety of reasons, from voltage control problems with automatic voltage regulators (AVR) and under-load tap-changer (ULTC) transformers, to instabilities created by different types of bifurcations. Several conference proceedings, e.g. [3, 4, 5], summarize most of the voltage stability problems and discuss techniques and models proposed by several researchers relating to the area of bifurcation theory.

Local bifurcations have been shown to cause system-wide voltage collapses and oscillatory problems in power networks [6, 7], leading in some cases to chaotic behavior of the corresponding mathematical model [6, 8]. These bifurcations are characterized by changes in the eigenvalues of the system equilibria as certain parameters change in the system. Typically, the generation or system loading levels are used as bifurcation parameters, which are varied slowly, moving the system from one equilibrium point to another. However, for certain values of the bifurcation parameter more com-

plicated behavior may result, leading to instability. Under these conditions it is possible for the system to exhibit oscillatory behavior [6], or even voltage collapse [7, 9]. These conditions are mathematically characterized by one of the system's eigenvalues becoming zero (saddle-node, transcritical, and pitchfork bifurcation), or by a pair of complex conjugate eigenvalues crossing the imaginary axis (Hopf bifurcation).

This thesis considers two related modeling issues in power system bifurcations studies. The first issue is to determine the effect of using different levels of model detail on system bifurcations and their corresponding effect on voltage collapse phenomena. Different models of induction motors, under-load tap-changing transformers, dynamic transmission line models, and dynamic lumped load impedances were considered. The number of eigenvalues of the system is increased as more system dynamics are considered. The behavior of these eigenvalues as the load is increased is then examined to determine if and when the system undergoes a bifurcation.

The study is motivated by determining which reduced dynamic induction machine model and system model adequately represent motor loads in voltage collapse studies. The second issue considers a generalized algorithm to remove nonlinear algebraic equations from the system model. In the current literature of bifurcation analysis, either the generator or the load are modeled using differential equations, but the transmission system is generally modeled using algebraic variables. A model for incorporating transmission line dynamics into bifurcation analysis is presented in [10], but the model can not be applied to all power system problems.

1.1 Literature Review

The importance of load modeling in voltage stability studies, especially in the location of the bifurcation points and the corresponding system dynamic response has been addressed in several studies, e.g., [7, 10, 11, 12, 13, 14, 15]. However, there has been little agreement in the power system community as to which particular load models are adequate for these types of studies. Various load models have been proposed in [16, 17, 18, 19, 20] to capture the basic dynamic voltage response of the load in the system.

In [11], the authors examine the characteristics of power systems where induction motors constitute a main portion of the load. In their study, three different induction motor load models are considered. The loads were modeled as constant, linear and quadratic functions of the induction motor rotor speed. Static loads were also included in the system model, allowing for the examination of the effect of changing the proportion of the total load which was composed of static elements. Fixed voltage, and constant power generator models were used, with no generator dynamics considered. The study found that for constant load models, saddle-node bifurcations occurred at higher voltage levels and at higher speeds as compared to the speed dependent mechanical load models. Furthermore, in a simple example, the percentage of the total load composed of induction motor load did not affect the nature of bifurcations, but did influence the value of induction motor loading at which the bifurcations occurred.

The effect on voltage collapse of combined induction motor and impedance loads by means of lab measurements and computer simulations using reduced load models is studied in [12]. The study focused on the issue of switching

capacitors to prevent voltage collapse in heavily loaded systems and the operation of induction motors on the lower portion of the power-voltage curve.

In [13, 14], the effect of modeling dynamics of under load tap changing transformers on voltage stability is studied. The studies used a continuous time model for tap changing for the system transformers, arguing that such a model is an acceptable approximation of discrete tap movements in studies of voltage collapse. The focus of the studies were to determine control strategy to lock the transformers tap changers to help prevent voltage collapse when the system is heavily loaded. The interaction between dynamics of under load tap changing transformers and loads were illustrated in their research, showing that such interaction plays a major role in bifurcations.

A Hopf bifurcations was detected, along with typical saddle-node bifurcations, in [15] with a simple two bus single generator system. The loads in the system were modeled using a third order induction motor model and lumped impedance elements. The system generator was modeled using a dynamic two-axis model with an IEEE type 1 Exciter. Transmission line models were not incorporated into the studies.

The use of dynamic transmission system models are presented in [10], with a simple single generator example. Although, in the study, load models were limited to resistive and inductive elements.

In the current literature, individual components of power systems have been examined in bifurcation studies, but little attention has been placed on the possible interaction of different system components. For example, [11] considers only detailed models of induction motors while approximating the remainder of the system with steady state models, and [10] considers

dynamic system transmission models but examined only simple loads. This gap motivated the research presented in this thesis.

1.2 Content

Chapter 2 of this study introduces the field of bifurcation analysis. Emphasis is placed on characteristics of saddle-node and Hopf bifurcations; the chapter is concluded with a review of methods used in the detection of bifurcations. Chapter 3 presents the models used in the thesis of the different components of the system, including the induction motor, synchronous generator, static loads, under-load tap-changing transformers, and the transmission line. In Chapter 4, bifurcation analysis is performed on a sample power system using several models, each incorporating different levels of modeling. Some of the basic concepts of bifurcation theory are also related back to well known concepts of motor stability through the use of torque-speed characteristics. A generalized algorithm to model a power system in which the algebraic equations are simple linear constraints is proposed in Chapter 5. Conclusions are presented in Chapter 6.

Chapter 2

Bifurcation Theory

Nonlinear phenomena such as Hopf and saddle node bifurcations have been shown to be responsible for some stability problems in power systems [21]. In stability analysis, differential-algebraic mathematical models of the power system are developed. These models are linearized at equilibrium points to determine the steady state stability using eigenvalue analysis. Of interest is where the system goes from being stable to unstable; from being unstable to stable; or where the number of equilibrium points change with respect to a bifurcation parameter. These bifurcations are mathematically characterized by one of the system eigenvalues becoming zero (saddle-node, transcritical and pitchfork bifurcation), or by a pair of complex conjugate eigenvalues crossing the imaginary axis (Hopf bifurcation).

The differential-algebraic equations used to model the power system model are of the form:

$$\dot{x} = f(x, y, \lambda) \tag{2.1}$$

$$0 = g(x, y, \lambda) \tag{2.2}$$

where $x \in \Re^n$ is a vector of the state variables, $y \in \Re^m$ is a vector of algebraic variables, and $\lambda \in \Re$ is any parameter in the system that changes slowly, moving the system from one equilibrium point to another. Equilibrium points are the values x_0, y_0, λ_0 where the rate of change of each state variable is zero, that is,

$$0 = f(x_0, y_0, \lambda_0) \tag{2.3}$$

$$0 = g(x_0, y_0, \lambda_0)$$

Equilibrium implies the system is at "rest" but does not imply stability. The stability and changes in the stability of a system is described throughout this chapter.

When the Jacobian $D_y g(\cdot)$ of the algebraic constraints in (2.2) is non-singular along system trajectories, the system model can be reformulated based on the Implicit Function Theorem [22] as:

$$y \equiv h(x, \lambda) \tag{2.4}$$

$$s(x, \lambda) \equiv F(x, h(x), \lambda) \tag{2.5}$$

$$\dot{x} = s(x, \lambda) \tag{2.6}$$

If the Jacobian of the algebraic constraints becomes singular then the model used to describe the system becomes invalid. In this case the original model

can be modified to consider dynamics ignored in the original model, resulting in the transformation of some algebraic constraints into differential equations [22]. This is discussed in greater detail in Chapter 5.

The outline of this chapter is as follows. First the characteristics of saddle-node bifurcations are presented. Then Hoft bifurcations are reviewed, with an introduction into solutions of limit cycles and evaluation of the stability of limit cycles. Finally, methods for the detection of bifurcations are reviewed.

2.1 Saddle-Node Bifurcations

Saddle-node bifurcations are characterized by two equilibrium points, typically one stable (s.e.p.) and one unstable (u.e.p.). These points merge at the equilibrium point (x_0, y_0) for the parameter value $\lambda = \lambda_0$; this equilibrium point has a simple and unique zero eigenvalue of $D_x s|_0$ [22, 1, 23]. If the two merging equilibria coexist for $\lambda < \lambda_0$, the two equilibrium points locally disappear for $\lambda > \lambda_0$, and vice versa.

Saddle-node bifurcations are well demonstrated using the following simple single variable example [1]. Consider

$$\dot{x} = \lambda - x^2 \tag{2.7}$$

where λ is the bifurcation parameter. The derivative of (2.7) is:

$$D_x s = -2x \tag{2.8}$$

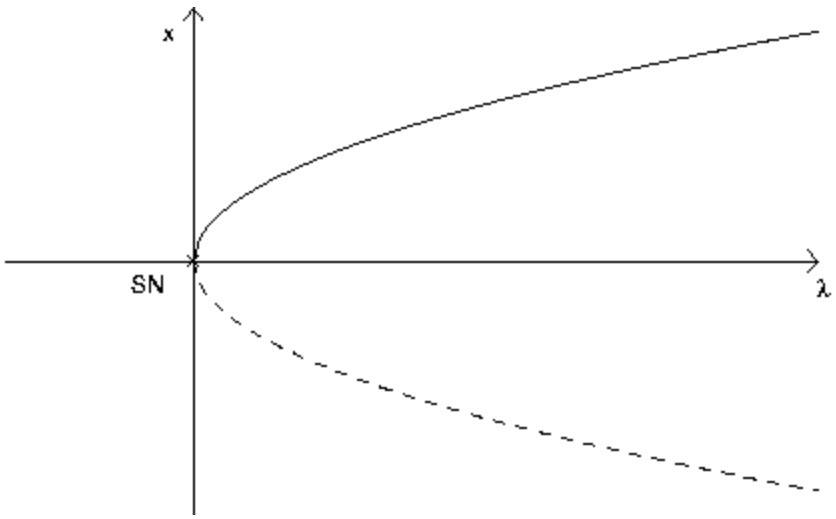

Figure 2.1: Bifurcation diagram of equation (2.7). The s.c.p.s are represented with a continuous line, whereas the u.c.p.s are depicted with a dotted line.

where s is the function given by the right hand side of equation (2.7) and D_x represents the derivative of this function with respect to x. The bifurcation diagram for this function is illustrated in Figure 2.1; stable equilibrium points exist on the upper portion of the graph and unstable points on the lower portion. Of interest is the equilibrium point located at the origin where the unstable and stable equilibrium points merge. This point is referred to as a saddle node bifurcation.

As illustrated, saddle node bifurcations are local bifurcations, occurring at the point where the equilibrium locally vanishes for further values of the bifurcation parameter. This does not exclude the possibility in more complex systems for there to exist equilibrium points for values of the bifurcation parameter beyond the saddle-node globally. A bifurcation diagram illustrating such a possibility is shown in Figure 2.2. At the point labeled $SN2$ there

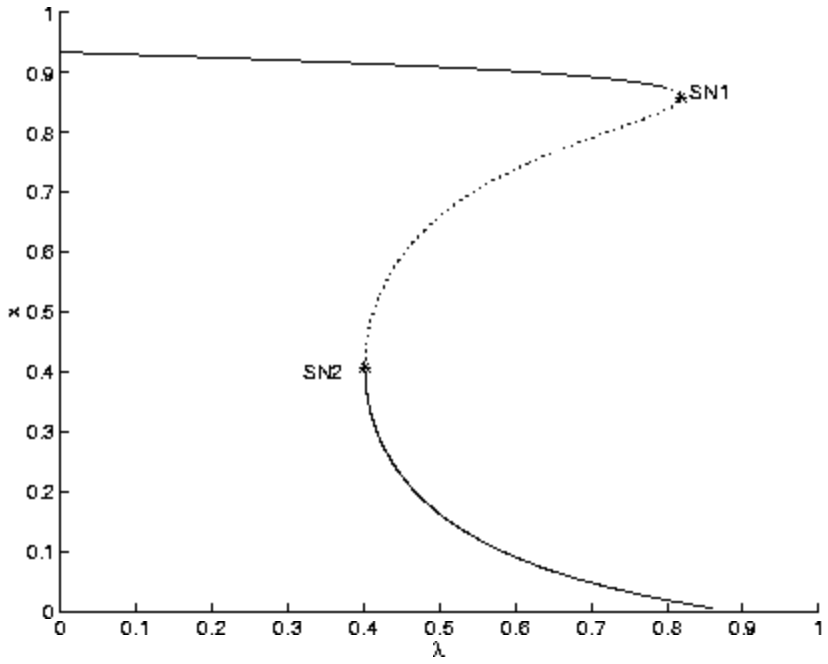

Figure 2.2: Bifurcation diagram of a multi-variable function. The s.c.p.s are represented with a continuous line, whereas the u.c.p.s are depicted with a dotted line.

are locally no equilibrium points for decreased values of λ. However, globally there exists an equilibrium for decreased values of λ along the top portion of the manifold. The multi-variable function used to create Figure 2.2 is based on a system discussed in Chapter 4.

The following conditions hold for saddle-node bifurcations [1]:

1. The point is an equilibrium point, i.e., $s(x, \lambda) = 0$.
2. The Jacobian of the function has one zero eigenvalue.
3. At the saddle-node two branches intersect and both disappear beyond the saddle-node.

Finally, saddle-node bifurcations are considered generic, that is they are expected to occur is power systems [21]. For example, if the loading of a power system was modeled as the bifurcation parameter λ, saddle-node bifurcations would be expected for certain values of λ.

2.2 Hopf Bifurcations

Hopf bifurcations have been shown to exist in several realistic power system models [9, 21, 22]; the Hopf bifurcations found in [9, 21, 22] occurred close to the "knee" of the PV curve. Therefore, if a Hopf bifurcation occurs in a power system, a minor load increase from this point might result in the system becoming unstable. This indicates that the oscillations associated with Hopf bifurcations in power systems may be very difficult to detect.

Hopf bifurcations do not yield any changes in the number of equilibrium points. These types of bifurcations are characterized by a complex conjugate

pair of eigenvalues, for the equilibrium point (x_0, y_0, λ_0), lying on the imaginary axis of the complex plane. When the parameter λ changes, the complex conjugate pair moves away from the imaginary axis, either to the right or to the left. In this case, stable or unstable limit cycles (system oscillations) appear or disappear. Depending on the stability of these limit cycles, the Hopf bifurcations can be either subcritical or supercritical [21, 22, 1].

The conditions of a Hopf bifurcation for a system modeled using a set of differential-algebraic equations (2.1) at an equilibrium point (x_0, y_0, λ_0), where $D_y g|_0$ is non-singular, are [21, 22, 1]:

1. $D_x s|_0$ has a simple pair of purely imaginary eigenvalues, and no other eigenvalue with zero real part.

$$\mu(\lambda_0) = \pm j\beta \tag{2.9}$$

   where $\mu(\lambda_0)$ represents the subset of the eigenvalues of the Jacobian of equation (2.6) which have purely imaginary values.

2. The purely imaginary eigenvalues cross the imaginary axis with "non-zero speed", i.e.,

$$\frac{dRe(\mu(\lambda_0))}{d\lambda} \neq 0 \tag{2.10}$$

The initial period of the zero-amplitude oscillation (limit cycle) is:

$$T_0 = \frac{2\pi}{\beta} \tag{2.11}$$

Depending on the stability of the limit cycle, the Hopf bifurcation can be classified as subcritical or supercritical. Supercritical bifurcations have

locally stable solutions on both sides of the bifurcation [1]. Therefore, a supercritical Hopf bifurcation will involved the exchange of stability between the stationary branch and the limit cycle. For the subcritical bifurcation there is a local loss of stability at the bifurcation point. Figures 2.3 and 2.4 illustrate these types of Hopf bifurcations.

2.2.1 Solutions of Limit Cycles

The periodic solution or limit cycle resulting from the Hopf bifurcation can be determined by solving the following boundary-value problem for $t\epsilon[t_0, t_0+T]$ [1],

$$\begin{bmatrix} \dot{x} \\ \dot{T} \end{bmatrix} = \begin{bmatrix} s(x,\lambda) \\ 0 \end{bmatrix} \tag{2.12}$$

$$\begin{bmatrix} x(t_0) - x(t_o+T) \\ p(x(t_0),\lambda) \end{bmatrix} = 0$$

Equation (2.12) is composed of two parts. The first part incorporates the original system's differential equations with the addition of the condition that the change in the period of the limit cycles must be zero. The second part incorporates the periodicity condition, which requires that after the period T, the system returns to its initial values. The second part also incorporates a phase condition, $p(x(t_0),\lambda)$, which is used to fix the initial moment, t_0.

The phase condition can be defined using several possible relations, for

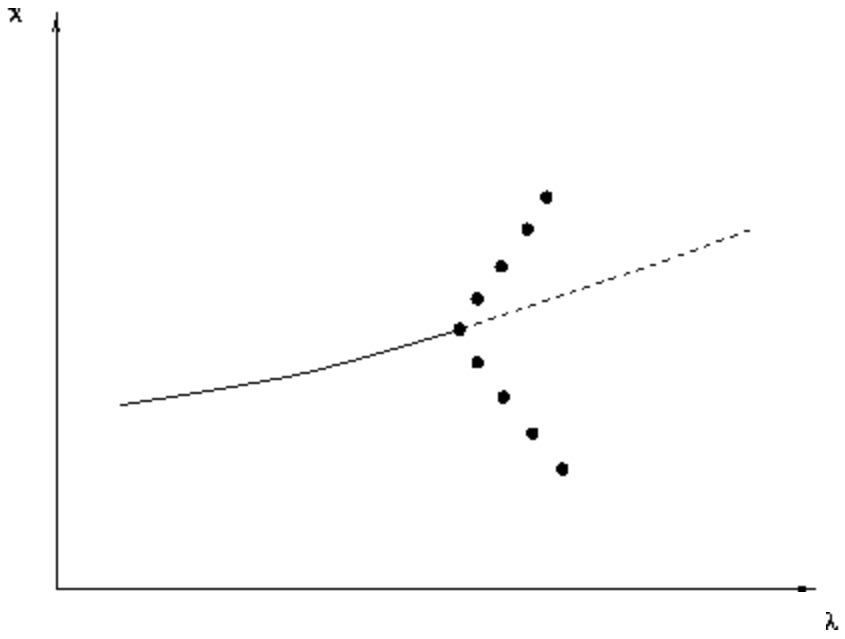

(a)

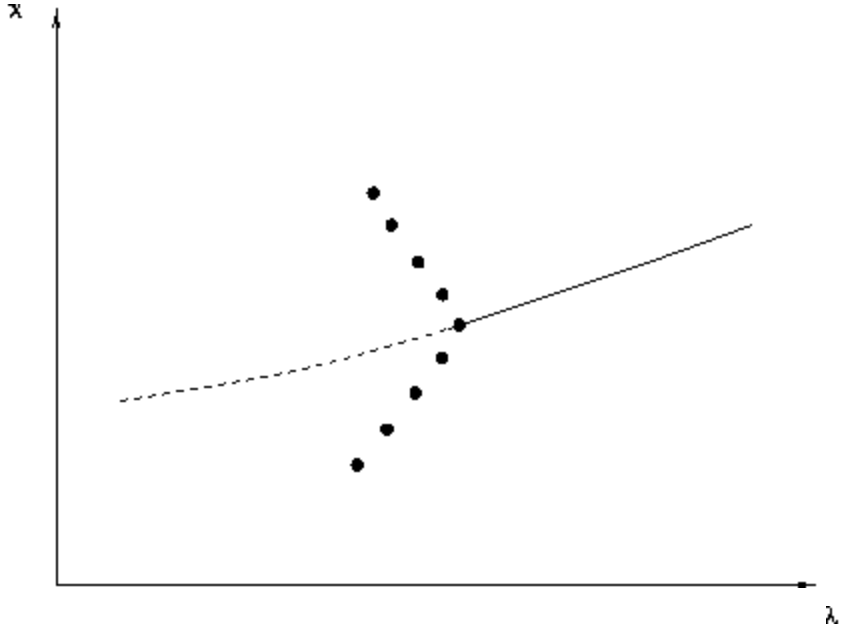

(b)

Figure 2.3: Supercritical Hopf bifurcation. Stable limit cycle amplitudes are depicted using solid circles

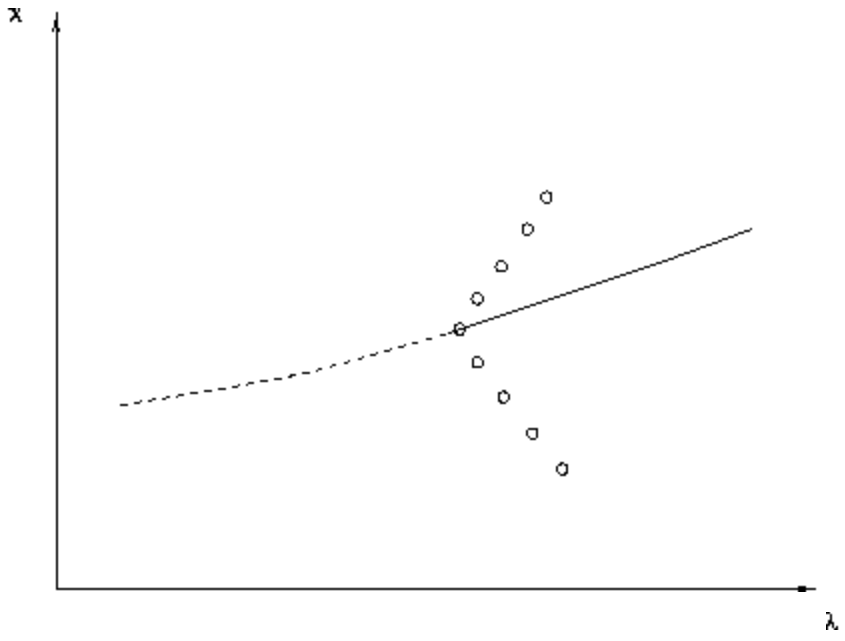

(a)

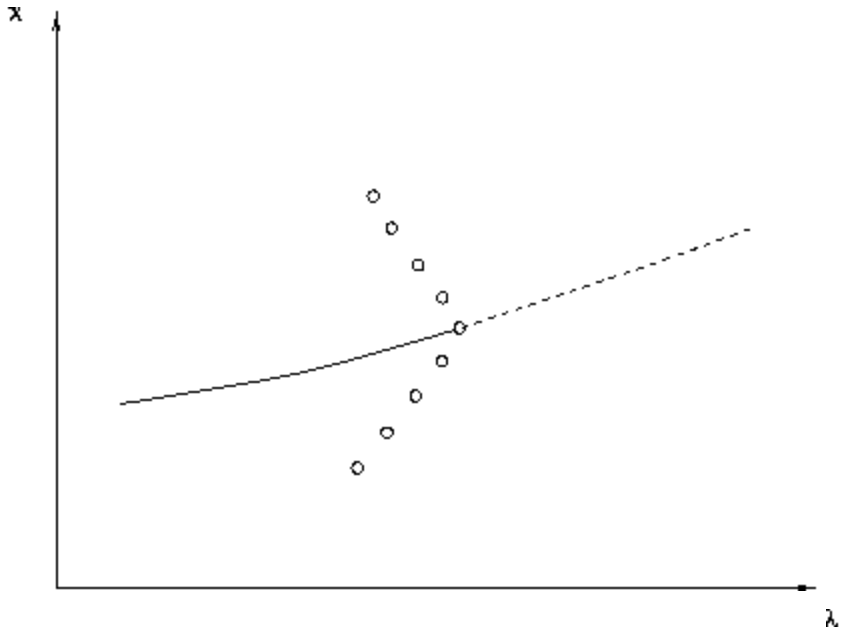

(b)

Figure 2.4: Subcritical Hopf bifurcation. Unstable limit cycle amplitudes are depicted using open circles.

example two possible relations are [1]:

$$p(x(t_0), \lambda) = x_k(t_0) - \eta = 0 \tag{2.13}$$

$$p(x(t_0), \lambda) = s_k(x(t_0), \lambda) = 0 \tag{2.14}$$

In (2.13) η is a fixed value in the range of $x_k(t)$. The phase condition given by (2.14) is advantageous, because it does not require previous knowledge of the solution range [21]. This condition does require that t_0 be a critical point, i.e., a local minimum or maximum of x_k.

The original problem can then be normalized to have a unit time length:

$$\begin{bmatrix} x' \\ T' \end{bmatrix} = \begin{bmatrix} Ts(x, \lambda) \\ 0 \end{bmatrix} \tag{2.15}$$

$$\begin{bmatrix} x(0) - x(1) \\ p(x(0), \lambda) \end{bmatrix} = 0$$

where the prime is used to indicate the variables have been normalized to the time interval $0 \leq t \leq 1$.

2.2.2 Stability of Limit Cycles [1]

The stability of the limit cycles describes the behavior of system trajectory located initially close to the limit cycle. If the cycle is stable, then the distance between the limit cycle and the original trajectory decreases. The

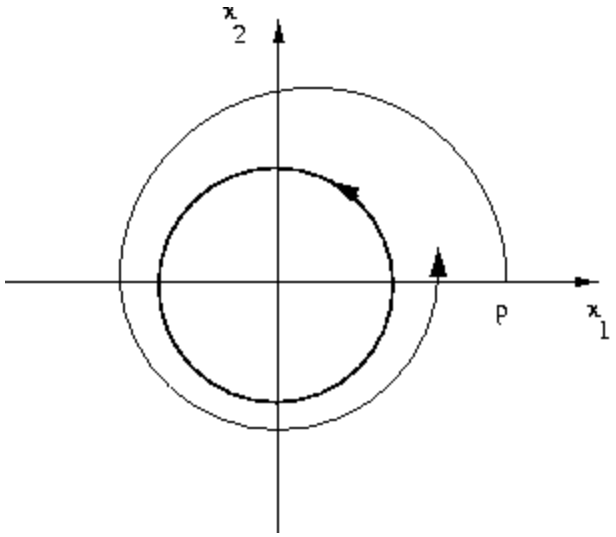

Figure 2.5: Illustration of stability of limit cycles

stability of limit cycles can be illustrated using Figure 2.5, which is based on a simple example presented in [1]. In this example, the inner circle represents the limit cycle of a two variable problem, $[x_1, x_2]$. Therefore, starting from the x_1 intercept of the limit cycle in the right hand plane, the solution will return to this point again after a period T. The same applies to any point on the inner circle. If the system is perturbed, to the point labeled p, the limit cycle is stable, if after each period T, the variables converge to the original limit cycle.

Mathematically, the trajectories of the system are denoted by ϕ, i.e.:

$$\phi(t : z) \text{ solves } \dot{x} = s(x, \lambda) \text{ with } x(0) = z \tag{2.16}$$

where z represents the original trajectory of the system, which can be variables in a neighboring trajectory of a periodic solution, z^*.

The distance between an arbitrary system trajectory and the limit cycle

is then given by:

$$d(t) = \phi(t : z^* + d_0) - \phi(t : z^*) \tag{2.17}$$

where $d(t)$ is the distance from the periodic solution z^* and the perturbed initial trajectory z.

A Taylor expansion of $d(t)$ after one period yields:

$$d(t) = \frac{\partial \phi(t : z^*)}{\partial t} d_0 + \text{ higher order terms} \tag{2.18}$$

The monodromy matrix, M_λ, which is the first term in the Taylor expansion of $d(t)$,

$$M_\lambda = \frac{\partial \phi(t : z^*)}{\partial t} \tag{2.19}$$

is critical in determining if the distance d will decrease after a finite length of time. Furthermore, M_λ will have one unity eigenvalue. The stability of the limit cycle can then be evaluated using Floquet theory:

1. If the moduli of all eigenvalues are less than 1, the associated limit cycle is stable (attracting).

2. If the modulus of at least one eigenvalue is larger than 1, the associated limit cycle is unstable (repelling).

These techniques require the system be of the form (2.6) which is typically not feasible when considering large power systems. Therefore, using the monodromy matrix to determine stability of limit cycles in power systems is not usually possible.

An alternative method to determine the stability of limit cycles is the use of numerical integration to perform time simulations. Starting from an initial trajectory close to a know limit cycle, the limit cycle is stable if the numerical integration results in the trajectory converging to the limit cycle. This method is advantageous since numerical integrations are inexpensive [21]. The method does require that the limit cycle be known in advance since non-converging system trajectories provide no information as to the location of cycles.

2.3 Bifurcation Detection Methods

Direct and continuation methods can be used to detect bifurcations [1]. Direct methods have been successfully applied to determine the exact location of saddle-nodes in power systems [24, 25]. However, these methods present serious numerical difficulties when used to locate Hopf bifurcations of differential-algebraic models [21]. Continuation methods, on the other hand, can be used in all cases to detect any type of bifurcation without great difficulties [21, 25, 26, 27].

Two methods were used to perform bifurcation analyses in the thesis. The first method used a continuation method developed in Matlab [28]. Numerical routines were developed to determine the Jacobian of the system at equilibrium points in order to evaluate the steady-state stability of the system. The second method uses a Fortran-based software package, Auto97 [29]. This package uses a combination of continuation and direct methods to perform bifurcation analysis.

2.3.1 Continuation Methods

The systems examined are modeled using differential algebraic equations (2.1) and (2.2). At equilibrium points, the left side of (2.1) must equal zero. Since the systems under study are strictly continuous, equations (2.1) and (2.2) become

$$\begin{bmatrix} \dot{x} \\ 0 \end{bmatrix} = \begin{bmatrix} f(x, y, \lambda) \\ g(x, y, \lambda) \end{bmatrix} = F(z, \lambda) \tag{2.20}$$

where F represents all the system equations and z represents a vector composed of both the differential and the algebraic states. When the algebraic variables can be directly substituted, equation (2.20) becomes (2.6)

$$\dot{x} = s(x, \lambda) \tag{2.21}$$

Continuation techniques are generally composed of two or three steps. The first part is a predictor step, the second is a corrector step while the third is a parameterization routine. The last step can be omitted in some algorithms. When using continuation methods to detect bifurcations and trace bifurcation diagrams the bifurcation parameter λ is usually used as the initial parameter p.

The predictor and corrector steps are illustrated in Figure 2.6. From an initial solution z_0, p_0, a predictor step Δx and change Δp of the parameter are determined. From the new point, $z_1 = z_0 + \Delta z$, a corrector routine is used to calculate the new equilibrium point, z_2. A parameterization is used to ensure the Jacobian used in the continuation method does not become

singular at a saddle-node bifurcation. Generally, in bifurcation analysis the parameter p will be the bifurcation parameter λ. A more detailed description of the three steps, based on [1, 30], follows.

Predictor Step

Given an initial operating point, the predictor step is determined by computing the tangent vector to the manifold at this point and a step length. Since the initial point is an equilibrium point:

$$0 = F(z, \lambda) \tag{2.22}$$

The continuation parameter has been set to the bifurcation parameter, i.e. $p = \lambda$ and, therefore,

$$D_z F(z_0, p)\frac{dz}{dp} = -\frac{\partial F}{\partial p}|_0 \tag{2.23}$$

$$\Delta p = \frac{k}{\parallel dz/dp \parallel} \tag{2.24}$$

$$\Delta z = \Delta p \frac{dz}{dp} \tag{2.25}$$

where $\frac{\partial F}{\partial p}|_0$ is the partial derivative of the system equations with respect to the parameter p, and $D_z s(x_0, p)$ is the system Jacobian calculated at the initial point. The constant k is user defined to control the initial size of the step.

Initially, the parameter p is set to the bifurcation parameter λ, but as the system approaches a saddle-node bifurcation, p is likely to change to one of

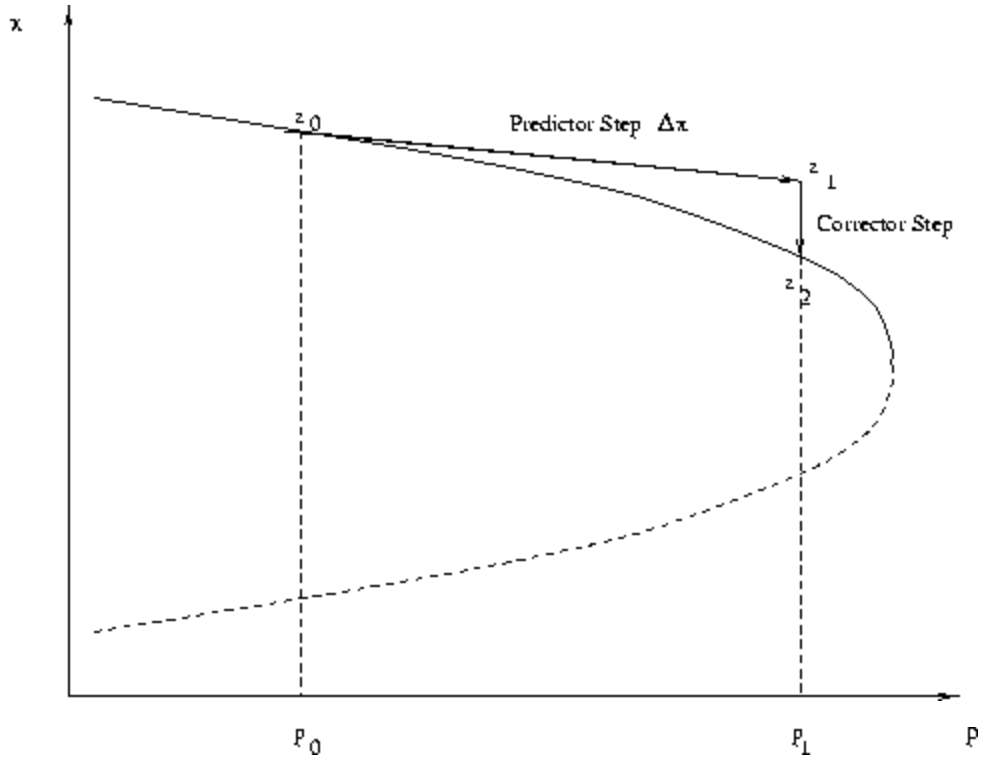

Figure 2.6: Illustration of continuation algorithm

the system voltages [30] as explained in the parameterization step. In [30] a value of $k = 1$ is recommended for good results. For the analysis presented a value of $k = 0.5$ was used to obtain more data points to generate the bifurcation diagram.

Once the steps Δz and Δp are determined, the new vector z_1 and parameter value p_1 are given by

$$z_1 = z_0 + \Delta z \tag{2.26}$$

$$p_1 = p_0 + \Delta p \tag{2.27}$$

Corrector Step

Using the new vector and parameter value found in the previous step, a corrector routine is used to find the intersection between the perpendicular plane to the tangent vector, at the new point z_1, and the systems solution manifold. This is found by solving the following equations

$$F(z, p) = 0 \tag{2.28}$$

$$\Delta p(p - p_0 - \Delta p) + \Delta z^T(z - z_0 - \Delta z) = 0 \tag{2.29}$$

where Δp and Δz are the solution of the predictor step. An initial guess for z and p as z_1 and p_1 respectively will usually result in good convergence [30]. If the algorithm is unable to converge to a solution, the steps Δp and Δz determined in the predictor algorithm are halved.

Parameterization Step

Parameterization is the optional step where the parameter p is changed to the variable that presents the largest change in the predictor step. This is determined as follows:

$$p \leftarrow max\left\{\left|\frac{\Delta\hat{z}_1}{\hat{z}_1}\right|, \left|\frac{\Delta\hat{z}_2}{\hat{z}_2}\right|, ..., \left|\frac{\Delta\hat{z}_n}{\hat{z}_n}\right|, \left|\frac{\Delta\hat{p}}{\hat{p}}\right|, \right\} \tag{2.30}$$

where n is the number of states in the system and the $\sim$ indicates that individual components of the vectors are considered, as identified by the subscript.

It is stated in [30] that the parameterization step will usually result in the bifurcation parameter being changed to one of the system bus voltages. Because of the highly nonlinear behavior of the Jacobian eigenvalues, references [25, 30] state that parameterization is not required to obtain good results when step cutting is incorporated into the Corrector step.

Once the continuation algorithm moves past a saddle-node bifurcation or turning point, the sign of Δp in equation (2.24) must be changed to trace to lower portion of the bifurcation diagram.

2.3.2 Successive Equilibrium Solution Method

A Newton-Raphson algorithm could be applied for incrementally increasing values of λ, the loading parameters. However, numerical difficulties can arise as the solution approaches a saddle node bifurcation, since at that point the Jacobian is singular. For typical power systems, the non-linear nature of the model is such that unless the system is rather close to the saddle-node

bifurcation, the Jacobian will not become numerically singular; therefore, a successive equilibrium method [25, 30] could be applied to obtain a solution close to the saddle-node bifurcation. Successive equilibrium methods solve the system equations for increasing values of the loading parameter, but are generally limited to the range of solutions from the initial point to the first saddle-node bifurcation.

2.4 Jacobian Computations

The eigenvalues of the Jacobian of the differential-algebraic model are used to evaluate the stability of the system at equilibrium points. As discussed in this chapter, the detection and evaluation of bifurcations is done using these eigenvalues. Two methods used to construct this Jacobian are reviewed in this section. The first method is the traditional method of forming the Jacobian from equations (2.1) and (2.2). The second method is based on numerical differentiation.

The system Jacobian can be calculated from equations (2.1) and (2.2) at each equilibrium point as follows:

$$J_s = D_x f|_0 \; - \; D_y f|_0 \; D_y g|_0^{-1} \; D_x g|_0 \tag{2.31}$$

The subscript 0 indicates that the function is evaluated at the equilibrium point described by equation (2.3).

Equation (2.31) has traditionally been used in stability studies but is numerically expensive to compute.

2.4.1 Numerical Differentiation

If equation (2.6) can be determined, then the Jacobian is defined as:

$$J_s = D_x s|_0 \tag{2.32}$$

The Jacobian $D_x s(x)$, can be numerically determined using a centered formula with Richardson's extrapolation. This extrapolation is a method to obtain an improved numerical approximation of a derivative using lower order approximations [31]. The numerical approximation improves as higher ordered centered formula are used. The familiar centered formula of second order for the derivative of a function is:

$$D_0(b) = \frac{s(x+b) - s(x-b)}{2b} \tag{2.33}$$

where b is a small step size and $D_i(b)$ is used to indicate the function is of order $2(i+1)$. In the approximation above, the error in the approximation is in the order of b^2.

The centered formula of fourth order for the derivative of a function is:

$$D_1(b) = \frac{-s(x+2b) + 8s(x+b) - 8s(x-b) + s(x-2b)}{12b} \tag{2.34}$$

In the approximation above, the error is in the order of b^4. The Richardson's Extrapolation states that an improved approximation to equation (2.34) has the form:

$$\frac{16D_1(b) - D_1(2b)}{15} \tag{2.35}$$

where $2b$ represents a doubling of the original step size. In the algorithm developed, each state, x was incremented using a value of $b = 10^{-5}$. A detailed description of these algorithms can be found in most numerical methods text books[31].

2.4.2 Numerical Jacobian Algorithm

As defined by equation (2.4), equation (2.6) is formulated by finding a function h such that:

$$y = h(x, \lambda) \tag{2.36}$$

But if numerical methods are being used, a closed form expression is not required, i.e., a numerical method can be applied at each equilibrium point to determine the values of the algebraic variables y, based on the value of the states x. The numerical method can be a simple Newton-Raphson algorithm.

When using numerical differentiation, small perturbations b are added to the equilibrium points as discussed in Section 2.4.1. A numerical equivalent of the close form expression $s(x, \lambda)$ of equations (2.1) and (2.2) is then found for any value of x. The Jacobian can then be formed using the numerical differentiation methods described in Section 2.4.1.

To illustrate the algorithm, the steps to determine the Jacobian using a second order formula is given.

1. Determine values for x_0, y_0, λ_0 at the equilibrium point.

2. To form each column of the Jacobian, perturb the state in x associate with the column by b, i.e, to form the first column, set $x^* = x_0 + \Delta x$ where Δx is a column vector with b in the first cell and the remaining cells set to zero.

3. Solve $g(x^*, y, \lambda)$ for y, i.e., numerically find $y = h(x^*, \lambda)$, where $x^* \in \Re^n$ is a vector formed by perturbing the state variables x as described above.

4. Using $F(x^*, h(x^*, \lambda), \lambda)$ calculate the $s(x+b, \lambda)$ term in equation (2.33).

5. Repeat steps 2-4 but perturb the respective state by $-b$ to calculate the $s(x-b, \lambda)$ term in equation (2.33).

6. Repeat steps 2-5 for all the states to form each column of the Jacobian.

In this thesis, the Jacobian $D_x s(x)$ was numerically determined using a fourth order centered formula with Richardson's extrapolation.

Chapter 3

System Modeling

To perform the bifurcation analysis proper models for the different components of the system were developed. These models are presented in this chapter for the induction motor, synchronous machine, ULTC transformer, transmission line, and impedance loads. To simplify the analysis, generalized reference frame models are used exclusively.

In this Chapter, first the generalized reference frame theory is introduced. Next the induction motor model is thoroughly discussed. The standard detailed model for the synchronous machine is also presented. Finally, models are given for the ULTC transformer, impedance loads, and transmission lines.

3.1 Generalized Reference Frame

Since the late 1920s when Park [32] first introduced his change of variables for the stator windings of a synchronous machine, the use of generalized reference frame transformations has simplified machine analysis. The gen-

eralized reference frame incorporates the separate reference transformations developed for induction and synchronous machines into one transformation model [33].

The transformation of the three phase rotor circuit variables to the generalized reference frame is [33]:

$$f_{qd0r} = K_r f_{abcr} \tag{3.1}$$

where $f^T_{qd0r} = [f_{qr} f_{dr} f_{0r}]$, $f^T_{abcr} = [f_{ar} f_{br} f_{cr}]$, the subscript r is used to represent parameters in the rotor, and

$$K_r = \frac{2}{3}\begin{bmatrix} cos(\beta) & cos(\beta - \frac{2\pi}{3}) & cos(\beta + \frac{2\pi}{3}) \\ sin(\beta) & sin(\beta - \frac{2\pi}{3}) & sin(\beta + \frac{2\pi}{3}) \\ \frac{1}{2} & \frac{1}{2} & \frac{1}{2} \end{bmatrix} \tag{3.2}$$

$$\beta = \Theta - \Theta_r \tag{3.3}$$

The angular displacements Θ and Θ_r are defined as:

$$\Theta = \int_0^t \omega(\zeta) d\zeta + \Theta(0) \tag{3.4}$$

$$\Theta_r = \int_0^t \omega_r(\zeta) d\zeta + \Theta_r(0) \tag{3.5}$$

where ω_r is the rotating speed of the circuit, i.e., the rotor speed. The angular displacement Θ is the displacement associated with the dq0 transformation's frame of reference. Therefore, the angular velocity, ω associated to the angular displacement Θ is unspecified; the frame of reference may have a constant or varying angular velocity.

The above transformation can be applied to rotor circuit parameters (induction motor, synchronous generator) or to stationary circuits (machines, transmission lines, impedance loads).

One advantage of reference frame transformations is the ability to eliminate time varying components. For example, considering a balanced three voltage source,

$$v_a = V_{mag}cos(\Theta_s) \tag{3.6}$$

$$v_b = V_{mag}cos(\Theta_s - \frac{2\pi}{3}) \tag{3.7}$$

$$v_c = V_{mag}cos(\Theta_s + \frac{2\pi}{3}) \tag{3.8}$$

Where V_{mag} is the peak voltage of the source, Θ_s is the angular position of the voltage defined using equation (3.9), ω_s is the frequency of the source.

$$\Theta_s = \int_0^t \omega_s(\zeta)d\zeta + \Theta_s(0) \tag{3.9}$$

Applying the transformation given in equation (3.1):

$$\begin{bmatrix} v_q \\ v_d \\ v_0 \end{bmatrix} = \begin{bmatrix} cos(\beta) & cos(\beta - \frac{2\pi}{3}) & cos(\beta + \frac{2\pi}{3}) \\ sin(\beta) & sin(\beta - \frac{2\pi}{3}) & sin(\beta + \frac{2\pi}{3}) \\ \frac{1}{2} & \frac{1}{2} & \frac{1}{2} \end{bmatrix} \begin{bmatrix} V_{mag}cos(\Theta_s) \\ V_{mag}cos(\Theta_s - \frac{2\pi}{3}) \\ V_{mag}cos(\Theta_s + \frac{2\pi}{3}) \end{bmatrix}$$

$$= \begin{bmatrix} V_{mag}cos(\Theta_s - \Theta) \\ -V_{mag}sin(\Theta_s - \Theta) \\ 0 \end{bmatrix} \tag{3.10}$$

When the angular velocity ω of the transformation is set equal to the frequency of the source ω_e, then the transformed voltages have constant values. The same analysis can be applied to any balanced three phase electrical variable (current, voltage, flux linkage).

3.1.1 dq0 Transformation on Resistive Elements

The application of the dq0 transformation to resistive elements is done by first considering the voltage across the resistors:

$$v_{abc} = Ri_{abc} \tag{3.11}$$

$$v_{qd0} = K_r R K_r^{-1} i_{qd0} \tag{3.12}$$

where

$$v_{qd0r}^T = [v_{qr} \;\; v_{dr} \;\; v_{0r}] \tag{3.13}$$

$$v_{abcr}^T = [v_{ar} \;\; v_{br} \;\; v_{cr}] \tag{3.14}$$

$$i_{qd0r}^T = [i_{qr} \;\; i_{dr} \;\; i_{0r}] \tag{3.15}$$

$$i_{abcr}^T = [i_{ar} \;\; i_{br} \;\; i_{cr}] \tag{3.16}$$

and R is a matrix with the resistance of each phase in the corresponding diagonal entries, and zeros in all other cells. The value of Θ_r is zero, for K_r defined in (3.2)-(3.5), since the rotational speed of the stationary circuit is zero. For stationary circuit, K_r is written as K_s to indicate $\Theta_r = 0$.

If the resistance of each of the phases is equal, then the nonzero elements of the matrix R are equal. Therefore, the resistive matrix is the same for

both the actual circuit and the arbitrary reference frame equivalent circuit since [33]:

$$K_s R K_s^{-1} = R \tag{3.17}$$

3.1.2 dq0 Transformation on Inductive Elements

For the inductive elements in the circuit:

$$v_{abc} = \frac{d}{dt}\psi_{abc} \tag{3.18}$$

$$v_{qd0} = K_s \frac{d}{dt}[K_s^{-1}\psi_{qd0}] \tag{3.19}$$

$$= K_s \frac{d}{dt}[K_s^{-1}]\psi_{qd0} + K_s K_s^{-1}\frac{d}{dt}\psi_{qd0} \tag{3.20}$$

$$= \omega_r \psi_{dq0} + \frac{d}{dt}\psi_{qd0} \tag{3.21}$$

where [33]

$$\psi_{dq0r}^T = [\psi_d \quad -\psi_q \quad \psi_0] \tag{3.22}$$

For linear systems, the relationship between flux linkage and current can be expressed as:

$$\psi_{abc} = L i_{abc} \tag{3.23}$$

$$\Rightarrow \quad \psi_{qd0} = K_s L K_s^{-1} i_{qd0} \tag{3.24}$$

If the circuit is such that there is no mutual inductance between phases and the self inductance of each of phases is equal, then L is a strictly diagonal matrix with equal non-zero diagonal elements:

$$K_s L K_s^{-1} = L \tag{3.25}$$

Typically in the analysis of machines, the inductance matrices used to relate the flux and the current can be written in the following two formats:

$$L_{s/r} = \begin{bmatrix} L_l + L_m & \frac{-1}{2}L_m & \frac{-1}{2}L_m \\ \frac{-1}{2}L_m & L_l + L_m & \frac{-1}{2}L_m \\ \frac{-1}{2}L_m & \frac{-1}{2}L_m & L_l + L_m \end{bmatrix} \tag{3.26}$$

$$L_{sr} = L_m \begin{bmatrix} cos(\Theta_r) & cos(\Theta_r + \frac{2\pi}{3}) & cos(\Theta_r - \frac{2\pi}{3}) \\ cos(\Theta_r - \frac{2\pi}{3}) & cos(\Theta_r) & cos(\Theta_r + \frac{2\pi}{3}) \\ cos(\Theta_r + \frac{2\pi}{3}) & cos(\Theta_r - \frac{2\pi}{3}) & cos(\Theta_r) \end{bmatrix} \tag{3.27}$$

where L_l and L_m are the leakage and magnetizing inductances, respectively. Equation (3.26) is used to represent the inductances in either the stator s or the rotor r of the machine. Equation (3.27) is used to represent the time varying inductances due to variations in the air-gap length while the machine is rotating. Applying the generalized transformation to (3.26),

$$K_s L_{s/r} K_s^{-1} = \begin{bmatrix} L_l + \frac{3}{2}L_m & 0 & 0 \\ 0 & L_l + \frac{3}{2}L_m & 0 \\ 0 & 0 & L_l \end{bmatrix} \tag{3.28}$$

Also, applying the dq0 transformation in the synchronous reference to the time varying inductance matrix it can be shown that[33]:

$$K_s L_{sr} K_s^{-1} = \begin{bmatrix} \frac{3}{2}L_m & 0 & 0 \\ 0 & \frac{3}{2}L_m & 0 \\ 0 & 0 & 0 \end{bmatrix} \tag{3.29}$$

Therefore, the application of the dq0 transformation on a symmetrical system effectively results in decoupled variables in the new reference frame and can remove the time varying impedances. The above analysis can be easily extended to capacitive elements.

If the load at a bus is modeled using static inductive elements shunted to ground, then equation (3.21) can be applied to model the dynamic behavior of the current in the inductive elements,

$$\begin{aligned} \dot{i}_{load_q} &= \frac{v_q}{L_{load}} - \omega i_{load_d} \\ \dot{i}_{load_d} &= \frac{v_d}{L_{load}} + \omega i_{load_q} \end{aligned} \tag{3.30}$$

where the d-axis and q-axis variables, d and q, respectively, include the inductor current i_{load} and the voltage at the load bus v; the subscript $load$ is used to indicate the variables are modeling loads. Equations (3.24) is used to redefine the flux linkage in terms of the current and inductance, while the zero sequence components are excluded since balanced conditions are assumed.

3.2 Induction Motor

Induction motors form a major portion of the loads in a power system [34], and often are referred to as the "workhorses" of industrial applications [35].

The induction motor was first invented by Nikola Tesla in 1886. The basic operation of the motor has remained the same since that time, although great enhancements in the efficiency, size and weight of the machine have been made. For example, in 1890 a 5-horsepower motor weighed approximately 1,000 pounds, where a modern 5-horse power motor can weigh 50 pounds [36].

One of the first engineering difficulties of the induction motor was the high frequency of the alternating-current power sources. After George Westinghouse acquired the rights to patents based on Tesla's work, Westinghouse engineers began to plan for 60 Hz sources, which allowed for widespread use of these motors. The major first American installation of induction motors was made at the Columbia Mills, S.C., in 1894, composed of four General Electric 65-horse power induction motors [36].

The mathematical model of the induction motor developed in this section starts with the basic machine equations using *abc* phase notation, then progresses to the generalized reference frame model [33, 34]. Reduced order models are then discussed.

3.2.1 Basic Operating Principals

A magnetic field, rotating at synchronous speed, is produced when a three phase set of voltages is applied to the stator. The speed of rotation of the magnetic field is given by:

$$n_s = \frac{120 f_e}{P} \tag{3.31}$$

where f_e is the system frequency and P is the number of poles.

The rotating magnetic field induces voltages in the rotor winding, due to the relative motion between the field and the rotor windings. The frequency of the induced voltage in the rotor (f_r) is a function of the relative velocities of the rotating field and the rotor. The induced voltage causes a current to flow in the rotor windings; the rotor current interacts with the rotating field to produce a torque, causing the rotor to accelerate. As the rotational speed of the rotor increases, the relative speed between the rotating field and the rotor decreases, reducing the magnitude of the induced voltage. As the relative motion approaches zero, the rotor induced voltages and currents also approach zero. Therefore, for an induction machine to operate as a motor, the rotating field speed must be greater than the rotor speed. The slip speed is defined as the difference between the stator rotating field speed and the rotor speed [37]:

$$n_{slip} = n_s - n_r \tag{3.32}$$

where n_r is the mechanical speed of the rotor and n_s is the stator rotating field speed. The slip speed expressed in per unit of the synchronous speed is:

$$s = \frac{n_s - n_r}{n_s} \tag{3.33}$$

The rotor voltage frequency is then given by:

$$f_r = s f_e \tag{3.34}$$

3.2.2 Basic Machine Model

The following basic equations and notation for the induction motor can be used to model the behavior of the machine [33, 34]. The mathematical model makes the following assumptions:

1. Infinite permeability of the iron
2. Radial flux density in the air-gap

Furthermore, the impact of the iron losses and slot effects are ignored.

The phase stator and rotor voltages are defined as:

$$\begin{aligned} v_a &= \frac{d\psi_a}{dt} + R_s i_a \\ v_b &= \frac{d\psi_b}{dt} + R_s i_b \\ v_c &= \frac{d\psi_c}{dt} + R_s i_c \end{aligned} \tag{3.35}$$

$$\begin{aligned} v_A &= \frac{d\psi_A}{dt} + R_r i_A \\ v_B &= \frac{d\psi_B}{dt} + R_r i_B \\ v_C &= \frac{d\psi_C}{dt} + R_r i_C \end{aligned} \tag{3.36}$$

where ψ is the flux linking the winding indicated by the subscript, R_s is the stator winding resistance and R_r is the rotor winding resistance. The subscripts ABC and abc indicate stator and rotor variables, respectively.

Using the standard *abc* phase reference the flux linkage is a function of the current as follows:

$$\begin{aligned}\psi_a =& L_{aa} i_a + L_{ab}(i_b + i_c) \\ &+ L_{aA}[i_A \cos(\Theta) + i_B \cos(\Theta + 120^\circ) + i_C \cos(\Theta - 120^\circ)]\end{aligned} \tag{3.37}$$

$$\begin{aligned}\psi_A =& L_{AA} i_A + L_{AB}(i_B + i_C) \\ &+ L_{Aa}[i_a \cos(\Theta) + i_b \cos(\Theta - 120^\circ) + i_c \cos(\Theta + 120^\circ)]\end{aligned} \tag{3.38}$$

where L_{ii} the flux linking the winding indicated by the subscript i, and L_{ij} is the inductance between windings i and j.

Under balanced conditions, or if no neutral winding exists, the vector sum of both the stator and the rotor currents must be zero:

$$\begin{aligned} i_a + i_b + i_c &= 0 \\ i_A + i_B + i_C &= 0 \end{aligned} \tag{3.39}$$

3.2.3 Machine Equations in the Generalized Reference Frame

Using the techniques described in the previous section the basic *abc* phase model can be transformed to different reference frames. As previously discussed, the synchronously rotating reference frame effectively removes mutual inductance and can transform time varying states into constant values. A synchronously rotating reference transformation also eliminates the time varying inductances in the induction motor model due to the variations in the air-gap length.

The stator and rotor voltages expressed in terms of d and q components are:

$$
\begin{aligned}
v_{ds} &= R_s i_{ds} + \frac{\omega_b}{\omega_e}\psi_{qs} + \frac{d\psi_{ds}}{dt}\frac{1}{\omega_b} \\
v_{qs} &= R_s i_{qs} - \frac{\omega_b}{\omega_e}\psi_{ds} + \frac{d\psi_{qr}}{dt}\frac{1}{\omega_b} \\
v_{dr} &= R_r i_{dr} + \frac{\omega_b - \omega_r}{\omega_e}\psi_{qr} + \frac{d\psi_{ds}}{dt}\frac{1}{\omega_b} \\
v_{qr} &= R_r i_{qr} - \frac{\omega_b - \omega_r}{\omega_e}\psi_{dr} + \frac{d\psi_{dr}}{dt}\frac{1}{\omega_b}
\end{aligned}
\tag{3.40}
$$

where

$$
\begin{aligned}
\psi_{qs} &= X_{ls} i_{qs} + X_m(i_{qs} + i_{qr}) \\
\psi_{ds} &= X_{ls} i_{ds} + X_m(i_{ds} + i_{dr}) \\
\psi_{qr} &= X_{lr} i_{qr} + X_m(i_{qs} + i_{qr}) \\
\psi_{dr} &= X_{lr} i_{dr} + X_m(i_{ds} + i_{dr})
\end{aligned}
\tag{3.41}
$$

where X_{ls}, X_{lr}, and X_m represent the stator and rotor leakage impedances and the machine mutual impedance, respectively. The stator s and rotor r variables v, i, and ψ stand for the dq voltages, currents, and flux linkages, respectively. The rotor speed is represented by ω_r, the base synchronous speed is $\omega_e = 2\pi 60$, and ω_b stands for the reference frame speed. The reference frame speed was set to the synchronous speed for the analysis performed.

The instantaneous power input to the stator using phase components is:

$$p_s = v_a i_a + v_b i_b + v_c i_c \tag{3.42}$$

In per unit, equation (3.42) in the dq0 reference frame becomes [33]:

$$p_s = v_{ds} i_{ds} + v_{qs} i_{qs} \tag{3.43}$$

The relationship between the mechanical and electrical torque in per unit is [33]:

$$T_e = 2H \frac{d\omega_r}{dt} \frac{1}{\omega_b} + T_l \tag{3.44}$$

where T_e corresponds to the electro-magnetic torque supplied to the machine, T_l corresponds to the mechanical torque output, and H represents the p.u. machine inertia. Equation (3.44) can be re-written expressing the electro-magnetic torque in terms of the stator flux leakage and current as follows:

$$\begin{aligned} \dot{\omega}_r &= \frac{\omega_b}{2H}(T_e - Tl) \\ &= \frac{\omega_b}{2H}(\psi_{ds} i_{ds} + \psi_{qs} i_{qs} - Tl) \end{aligned} \tag{3.45}$$

Using equations (3.45) and (3.40), a fifth order model of the induction motor may be formed. If reduced order models are considered, differential terms in equation (3.40) are set to zero, transforming differential equations into algebraic constraints. If the stator flux linkage transients are ignored, i.e., $\dot{\psi}_{qs} = \dot{\psi}_{ds} = 0$, the model is reduced to a third order model. Furthermore, if the rotor flux linkage transient terms are also ignored, i.e., $\dot{\psi}_{qr} = \dot{\psi}_{dr} = 0$, the model is reduced to a first order model with only one differential

equation that simulates the mechanical dynamics. Finally, by eliminating all differential terms in equations (3.40) and (3.45), the induction motor is reduced to a simple steady state model represented by impedances for a constant slip s.

3.3 Synchronous Machines

The following basic equations and notation for the synchronous motor are used to model the behavior of the machine [33, 34]. The stator and rotor voltages expressed in terms of d and q components are described as:

$$v_{qs} = -R_s i_{qs} + \frac{\omega_r}{\omega_e}\psi_{ds} + \frac{1}{\omega_e}\frac{d\psi_{qs}}{dt} \tag{3.46}$$

$$v_{ds} = -R_s i_{ds} - \frac{\omega_r}{\omega_e}\psi_{qs} + \frac{1}{\omega_e}\frac{d\psi_{ds}}{dt} \tag{3.47}$$

where the stator s and rotor r variables v, i, and ψ stand for the dq voltages, currents, and flux linkages, respectively. The stator winding resistance is R_s.

The 0 axis is ignored as the systems under study are assumed to be balanced. The damper windings of the machine are modeled with two damper windings in the q-axis and one in the d-axis of the rotor. The differential equations used to describe the dynamics of the flux in these windings are given as:

$$v_{kq1} = R_{kq1} i_{kq1} + \frac{1}{\omega_b}\frac{d\psi_{kq1}}{dt} \tag{3.48}$$

$$v_{kq2} = R_{kq2} i_{kq2} + \frac{1}{\omega_b}\frac{d\psi_{kq2}}{dt} \tag{3.49}$$

$$v_{kd} = R_{kd} i_{kd} + \frac{1}{\omega_b}\frac{d\psi_{kd}}{dt} \tag{3.50}$$

where the two q-axis damper windings are represented by $kq1$ and $kq2$, and the d-axis damper winding by kd, variables v, i, ψ, and R stand for the dq voltages, currents, flux linkages and winding resistance, respectively.

The relation between the flux and the current for the stator and rotor windings is as follows:

$$\begin{aligned}
\psi_{qs} &= -X_q i_{qs} + X_{mq} i_{kq1} + X_{mq} i_{kq2} \qquad (3.51)\\
\psi_{ds} &= -X_d i_{ds} + X_{md} i_{fd} + X_{md} i_{kd}\\
\psi_{kq1} &= -X_{mq} i_{qs} + X_{kq1} i_{kq1} + X_{mq} i_{kq2}\\
\psi_{kq2} &= -X_{mq} i_{qs} + X_{mq} i_{kq1} + X_{kq2} i_{kq2}\\
\psi_{fd} &= -X_{md} i_{ds} + X_{fd} i_{fd} + X_{md} i_{kd}\\
\psi_{kd} &= -X_{md} i_{ds} + X_{md} i_{fd} + X_{kd} i_{kd}
\end{aligned}$$

The reactances X_q and X_d are referred to as q- and d-axis reactances respectively [33], while the mutual and the linkage reactances for each winding are denoted by X_m and X_l, respectively.

The behavior of the flux generated by the field winding is modeled using equation (3.52). The automatic voltage regulator, which is described by equation (3.53), adjusts the magnitude of the field voltage to control the magnitude of the terminal voltage without droop.

$$v_{fd} = R_{fd} i_{fd} + \frac{1}{\omega_b} \frac{d\psi_{fd}}{dt} \qquad (3.52)$$

$$\dot{v}_{fd} = \frac{1}{T_a}(V_{ref} - V_t) \qquad (3.53)$$

where T_a is the time constant of the AVR, V_{ref} is a reference signal, and V_t is the magnitude of the generator terminal voltage. The magnitude of terminal voltage is expressed in terms of the stator q-axis and d-axis voltages as follows:

$$V_t = \sqrt{v_{qs}^2 + v_{ds}^2} \tag{3.54}$$

The final two dynamic variables in the synchronous machine model is the rotor speed and the governor. They are used to regulate the speed of the rotor, and, therefore, the frequency of the network. The governor operates by controlling the mechanical input power to the generator. No droop was introduced into the governor model to better match the steady state models of the generator, allowing for a better comparison of the different models of the system.

In order to define the rotor speed and governor dynamics the electrical power output must be defined. First, the instantaneous power input to the stator using phase components is given by:

$$p_t = v_a i_a + v_b i_b + v_c i_c \tag{3.55}$$

In per unit d-q components equation (3.55) becomes [33]:

$$p_t = v_{ds} i_{ds} + v_{qs} i_{qs} \tag{3.56}$$

The relationship between the mechanical and electrical torque, in per unit, which describes the dynamic behavior of the rotor, is given in equation

(3.57). The dynamic behavior of the speed is a function of a mismatch in the electrical output power and the mechanical input power. When a mismatch occurs, there is a power transfer between the rotor and the network.

$$T_e = \frac{2H}{\omega_e}\frac{d}{dt}\omega_r + T_m \tag{3.57}$$

T_e corresponds to the electro-magnetic torque generated by the machine, T_m corresponds to the mechanical torque applied at the shaft, and H represents the p.u. machine inertia. The rotor speed and synchronous speed are given by ω_r and ω_e respectively. Finally, to clearly represent the dynamics of the rotor speed equation (3.57) can be re-written as [33]:

$$\begin{aligned}\dot{\omega}_r &= \frac{\omega_b}{2H}(T_e - T_m) \\ &= \frac{\omega_b}{2H}(\psi_{ds}i_{ds} + \psi_{qs}i_{qs} - T_m)\end{aligned} \tag{3.58}$$

The behavior of the governor is given in equation (3.59). The governor operates on the principal that changes in the operating frequency indicates a power mismatch.

$$\dot{P}_m = \frac{1}{T_g}(\omega_{ref} - \omega_r) \tag{3.59}$$

where ω_{ref} is a reference speed, set to the desired output angular velocity and T_g is the time constant of the governor. The mechanical power P_m is related to the mechanical torque T_m as follows:

$$P_m = \omega_r T_m \tag{3.60}$$

Although the model used in the analysis was simple, its purpose was only to demonstrate the general effect of the governor on the system. More detailed governor models are presented in [33, 37, 38].

3.4 Under-Load Tap-Changing Transformer Model

The ULTC is assumed to be an ideal device, i.e. saturation and losses are neglected and any internal reactance is lumped into the transmission line impedance. The following equations were used to model the behavior of the ideal ULTC:

$$\begin{aligned} V_2 &= aV_1 \\ \dot{a} &= \frac{1}{T_t}(V_{2_0} - V_2) \end{aligned} \tag{3.61}$$

where a stands for the tap shift on the secondary side with respect to a nominal 1 p.u. value, V_{2_0} is the control set point, V_1 and V_2 are the voltage magnitudes of the primary and secondary busses, respectively, and T_t represents the ULTC time constant.

To simplify the analysis of the aggregated load while retaining some of the important voltage control features of the ULTC, the model assumes a continuous control with no limits. However, in practise tap changing would

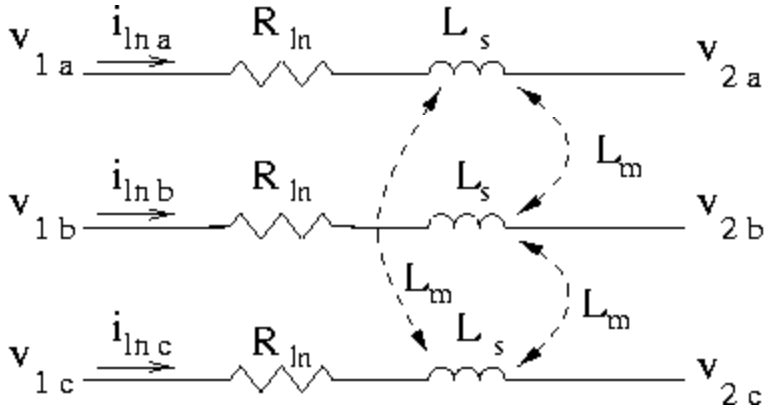

Figure 3.1: Single Line Diagram of Transmission Line

occur in discrete steps. The use of a continuous representation has been shown to provide useful results in previous investigations [9, 13, 39].

3.5 Transmission Line

The reference frame transformation presented in Section 3.1 can be easily extended to the transmission line model. As with the other elements of the system, the transmission line is modeled in the d-q-axis.

Applying Kirchhoff's voltage law to the single line diagram in Figure 3.1 gives:

$$v_{1a} - v_{2a} = v_{aR} + v_{aL} \tag{3.62}$$

$$v_{1b} - v_{2b} = v_{bR} + v_{bL}$$

$$v_{1c} - v_{2c} = v_{cR} + v_{cL}$$

(3.63)

where the *abc* subscripts refer to the individual phases and the voltage across the resistor and inductor are represented by v_R and v_L, respectively.

Similarly, in the dq0 reference frame,

$$v_{1q} - v_{2q} = v_{qR} + v_{qL} \tag{3.64}$$

$$v_{1d} - v_{2d} = v_{dR} + v_{dL}$$

$$v_{10} - v_{20} = v_{0R} + v_{0L}$$

where the *dq0* subscripts refer to variables in the d,q, and 0 axes respectively and the voltage across the resistor and inductance is represented by v_R and v_L, respectively.

From equation (3.12), the voltage across the resistor in the dq0 reference frame is:

$$
\begin{aligned}
v_{qR} &= R_{ln} i_q \\
v_{dR} &= R_{ln} i_d \\
v_{0R} &= R_{ln} i_0
\end{aligned}
\tag{3.65}
$$

where R_{ln} is the per unit resistance of each line.

In Section 3.1.1, equations (3.21) describes the voltage across three phase inductive elements in the dq0 axis. Since the transmission line inductance matrix is the same form as the matrix given in equation (3.26), equation (3.28) can be used to evaluate $K_s L_s K_s^{-1}$. The relationship between the flux linkage and the current is described by the matrix L_s. Therefore,

$$
K_s L_s K_s^{-1} = \begin{bmatrix} L_s - L_m & 0 & 0 \\ 0 & L_s - L_m & 0 \\ 0 & 0 & L_s + 2L_m \end{bmatrix}
\tag{3.66}
$$

where the self and mutual inductances is represented by L_s and L_m respectively. Therefore, the transmission line is modeled in the dq0 reference as:

$$
\begin{aligned}
v_{1q} - v_{2q} &= R_{ln} i_q + \omega \psi_q + \frac{d}{dt} \psi_q \\
v_{1d} - v_{2d} &= R_{ln} i_d - \omega \psi_d + \frac{d}{dt} \psi_d \\
v_{10} - v_{20} &= R_{ln} i_0 + \frac{d}{dt} \psi_0
\end{aligned}
\tag{3.67}
$$

where the flux linkages are expressed in terms of the impedances as

$$\begin{aligned} \psi_q &= (L_s - L_m) i_q \\ \psi_d &= (L_s - L_m) i_d \\ \psi_0 &= (L_s + 2L_m) i_0 \end{aligned} \tag{3.68}$$

Since the systems under study are assumed to be balanced, the 0-axis components can be removed. Therefore, the equations describing the dynamic behavior of current between two connecting buses is written as:

$$\begin{aligned} L_{ln} \frac{di_q}{dt} &= v_{1_q} - R_{ln} i_{ln_q} - \omega L_{ln} i_{ln_d} - v_{2_q} \\ L_{ln} \frac{di_d}{dt} &= v_{2_d} - R_{ln} i_{ln_d} + \omega L_{ln} i_{ln_q} - v_{2_d} \end{aligned} \tag{3.69}$$

where ω is the dq0 transformation reference frame speed, and $L_{ln} = L_s - L_m$.

Chapter 4

Bifurcation Analysis

Numerical simulations were performed on a typical power system based on a system extracted from [9, 2] and shown in Figure 4.1. The system load is composed of 5 large induction motors of 5,600 HP (1, 3 and 4) and 1,600 HP (2 and 5), plus 5 distribution transformers and transmission lines. Each induction motor is assumed to have an additional impedance load connected at its terminals. The generator on Bus 10 is used to model a typical source; the ULTC transformer is included to allow the system model to better imitate a typical supply scheme. The system is assumed to be balanced.

Using the techniques described in [40], the load was aggregated to reduce the system to the model depicted in Figure 4.2. The aggregate load is composed of a single induction motor and a static impedance load. The models used to represent the different components of the system are described in detail in Chapter 3.

Several software packages were used to obtain the results depicted in the following sections. Of these packages, AUTO97 [29] was used to determine

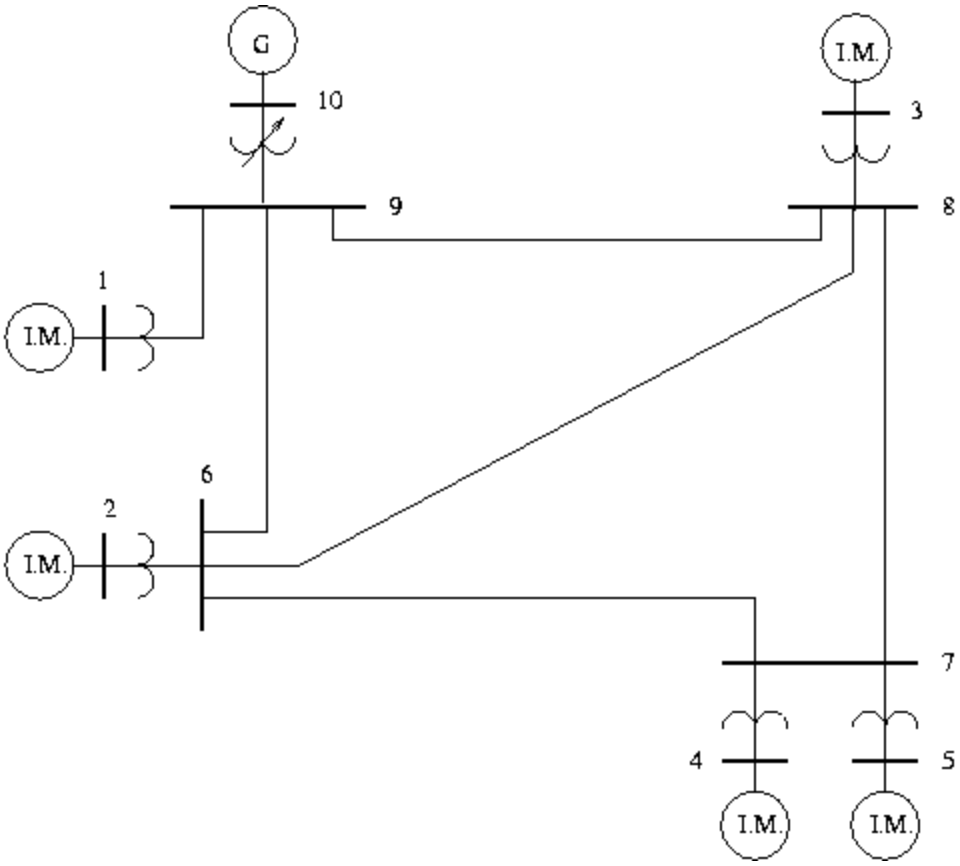

Figure 4.1: Example of a realistic power system load from [2].

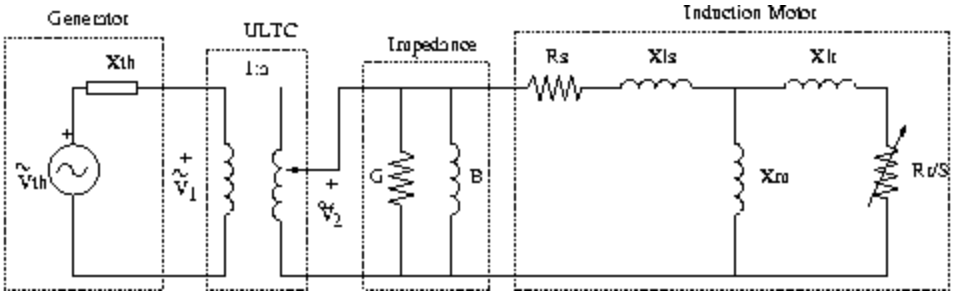

Figure 4.2: Aggregated load model for the test system of Figure 4.1. The generator is modeled with a simple Thevenin equivalent to represent the supply power system.

locations and types of bifurcations, especially in the case of Hopf bifurcations where determining stability of limit cycles is a difficult numerical problem [21]. Several Matlab based routines were also developed to validate the equilibrium points obtained from AUTO97 and to better illustrate eigenvalue characteristics.

The bifurcation analysis was performed on several variations of the system model, i.e., using different levels of detail. For example, the first system examined has only the induction motor and the ULTC transformer modeled with differential equations; this model results in a sixth order system model. The most detailed model uses differential equations to model the transmission line, the impedance and induction motor load, and the synchronous generator. The effect of parameter variation on the formation of bifurcations

is also examined.

The objectives of the analysis presented in this Chapter are focused on modeling issues in bifurcation analysis. Comparisons of the results of the different models can determine the appropriate level of modeling required to capture the most relevant features needed for bifurcation analysis; this is especially useful for voltage collapse studies. Because of the nature of a power system, different components and parts of individual components have different dynamical responses. The time constant associated with the components and their interactions influence the formation of bifurcations. These effects are examined by comparing different models of the induction motor load and the system, therefore, demonstrating appropriate levels of detail required in similar studies. A secondary objective raised in this Chapter is the issue of modeling transmission systems using dynamic equations. The objective was to remove all nonlinear algebraic equations from the model, thereby eliminating the possibility of the algebraic equations becoming singular [41], as discussed in detail in Chapter 5.

4.1 Generic Bifurcations

Saddle-node and Hopf bifurcations are generic, i.e., expected to occur, in power system models [22]. For example, the presence of saddle-node bifurcations in power systems with induction motor loads can be illustrated using the steady state torque characteristics for a 10 hp, 60 Hz induction motor with a mechanical load torque simulated as a linear function of the rotor speed. The parameters of the motor are extracted from [33] and are listed in

Table 4.1.

The mechanical load torque T_l is simulated as a linear function of the rotor speed as follows:

$$T_l = \frac{\lambda}{\omega_e}\omega_r \tag{4.1}$$

The bifurcation parameter λ has been incorporated into the model as a loading parameter to represent the loading factor of the induction motor. Equation (4.1) is a linear function of the rotor speed ω_r, which is defined as a function of the machine slip s as follows:

$$\omega_r = \omega_e(1-s) \tag{4.2}$$

The steady state characteristic of the induction motor is given by equation (4.3), where the induction motor is supplied by a voltage source with constant magnitude and frequency.

$$T_e = \frac{\frac{\omega_s}{\omega_e}X_m^2 R_r s V_t}{\left[R_s R_r + s\left(\frac{\omega_s}{\omega_e}\right)^2(X_m^2 - X_{ss}X_{rr})\right]^2 + \left(\frac{\omega_s}{\omega_e}\right)^2(R_r X_{ss} + s R_s X_{rr})^2} \tag{4.3}$$

where $X_{ss} = X_{ls} + X_M$, $X_{rr} = X_{lr} + X_M$, ω_e is the base synchronous speed, and ω_s is the system frequency, fixed at the base synchronous speed as a results of the Thevenin source.

A requirement of the system is that at equilibrium points the electromagnetic torque T_e and the mechanical load T_l are of equal magnitude. Therefore, system equilibrium points occur at the points of intersection of the

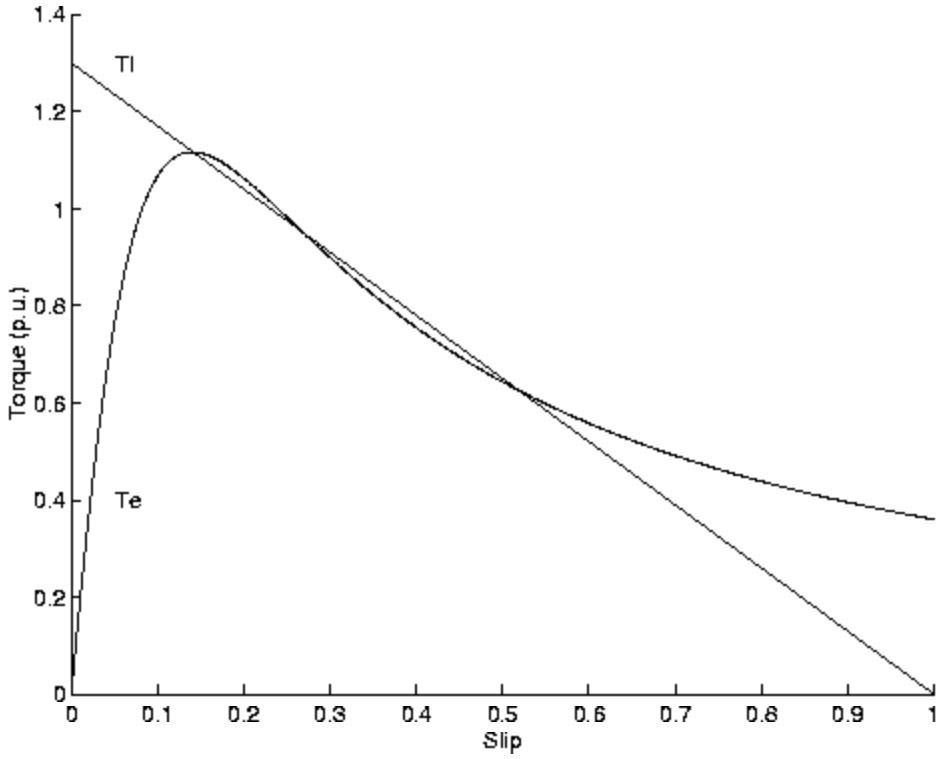

Figure 4.3: Steady state torque characteristics of the sample induction motor and mechanical load, for $\lambda = 1.3$.

Table 4.1: 6-pole, 220-volt, 10 Hp, 60 Hz Induction Motor

Variable	Value
r_s	0.0453 pu
X_m	2.042 pu
r_r	0.0222 pu
X_{ls}	0.1275 pu
X_{lr}	0.0322 pu
H	0.5000 sec.
V_t	1.0000 pu

two curves in Figure 4.3. The number of intersections between the two curves represents the number of equilibrium points for a given value of λ. As λ varies the number of intersections between the curves changes twice, indicating the presence of two saddle-node bifurcations. In Section 2.1, saddle-node bifurcations are characterized by merging equilibria, such that if equilibria exist for $\lambda < \lambda_0$, the two equilibrium points locally disappear for $\lambda > \lambda_0$, and vice versa. Therefore, Figure 4.3 demonstrates the presence of saddle-node bifurcations when the number of intersections of the curves change locally. The two cases are illustrated in Figure 4.4.

The value of λ for which the mechanical load intersects the maximum of the electro-magnetic torque curve represents the maximum loading of the system; this point is typically corresponds to the "knee" of the system power-voltage curve (PV curve). For the linear torque model used in this system, the number of intersections of the electro-magnetic torque curve and the mechanical load curve changes from 3 to 1 shortly after the maximum of the

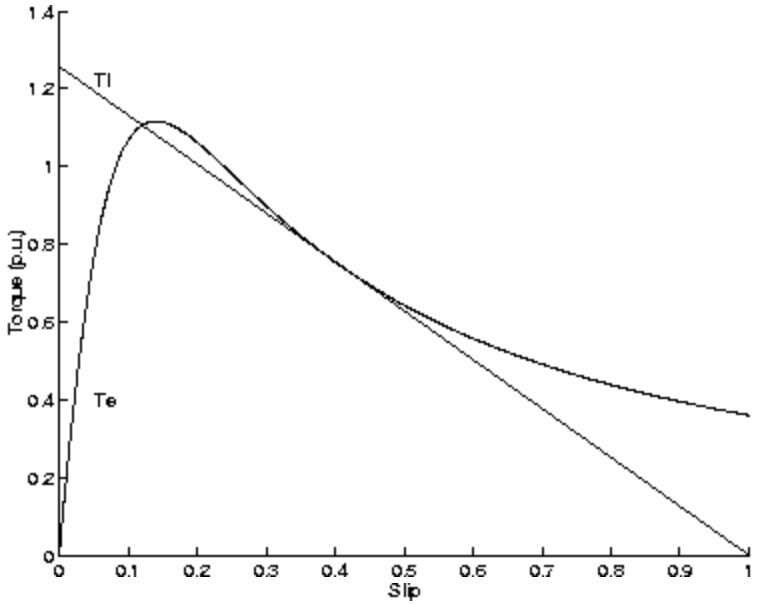

(a) $\lambda = 1.258$

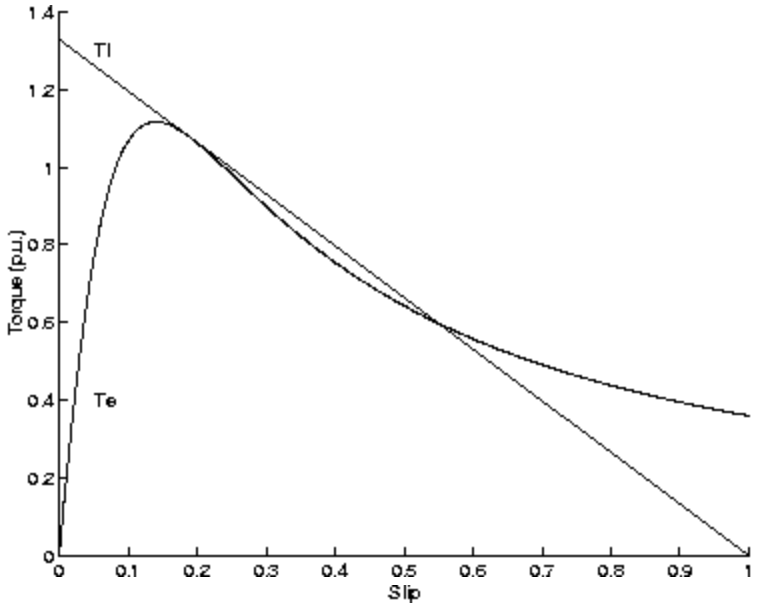

(b) $\lambda = 1.329$

Figure 4.4: Two saddle-node bifurcation cases for the sample induction motor and mechanical load.

electro-magnetic torque curves, i.e., a saddle-node bifurcation occurs close to the knee of the PV curve, at the lower half of the curve. If a constant torque model were used, the number of crossings between the two curves would change at the maximum of the electro-magnetic torque curve. This indicates that a saddle-node would occur on the knee of the PV-curve. A detailed examination of the effect of using different load models can be found in [11], which examines not only the number of bifurcations that occur but also the voltage profiles before the occurrence of the first bifurcation.

4.2 Detailed Induction Motor and ULTC Model

The bifurcation analysis was first performed on the system with only the induction motor and the ULTC transformer modeled with differential equations. The transmission line, impedance load, and the generator are modeled with strictly algebraic models.

The equivalent generator was modeled with a simple Thevenin circuit, to gain insight into the load behavior without complex generator models. In this model the generator was used as the system reference, i.e. $\widetilde{V}_{th} = V_{th}\angle 0^0$. Thus, the active and reactive powers P and Q delivered by the generator at the ULTC terminals are described by the following equations, where $\widetilde{V}_1 = V_1\angle\delta_1$:

$$\begin{aligned} P &= \frac{V_{th}V_1}{X_{th}}\sin\delta_1 \\ Q &= \frac{V_1^2}{X_{th}} - \frac{V_{th}V_1}{X_{th}}\cos\delta_1 \end{aligned} \tag{4.4}$$

The Thevenin impedance of the generator model is X_{th}, which incorporates the impedance of the transmission line, transformer and any internal generator impedances.

The real and reactive power being injected at the ideal ULTC from the Thevenin source is equal to the real and reactive demand of the load:

$$\begin{aligned} P &= V_2^2 G + P_{IM} \\ Q &= V_2^2 B + Q_{IM} \end{aligned} \tag{4.5}$$

where P_{IM} and Q_{IM} represent the real and reactive powers absorbed by the machine component of the load, and $V_2^2 G$ and $V_2^2 B$ represent the real and reactive powers absorbed by the static impedance component of the load.

The induction motor is described by equations (3.40), (3.41) and (3.45) in Chapter 3, whereas the ULTC Transformer is represented by (3.61). The mechanical load torque T_l is modeled as a linear function of the rotor speed as follows:

$$T_l = \frac{\lambda}{\omega_e}\omega_r \tag{4.6}$$

Equations (3.40), (3.41), (3.45), (3.61), (4.4), (4.5), and (4.6) were simulated in AUTO97 in order to detect bifurcations for the test system in Figure 4.2 for the parameter values given in Table 4.2.

Figures 4.5 through 4.8 depict the equilibrium points (stable and unstable) and bifurcations for the fifth order induction motor model. The load varies with changes in the mechanical torque parameter λ. Figure 4.5 shows two saddle-node bifurcations at $k_{SN_1} = 0.572672$ and $k_{SN_2} = 0.281250$, and

Table 4.2: Aggregated Load Data (100MVA, 4KV Base)

Variable	Value
R_s	0.07825 pu
X_{ls}	0.8320 pu
X_m	16.48 pu
R_r	0.1055 pu
X_{lr}	0.8320 pu
H	0.1836 s
ω_e	$2\pi 60$ s^{-1}
G	0.06047 pu
B	0.03530 pu
X_{th}	0.2 pu
T_t	5 s
V_{2_0}	1 pu

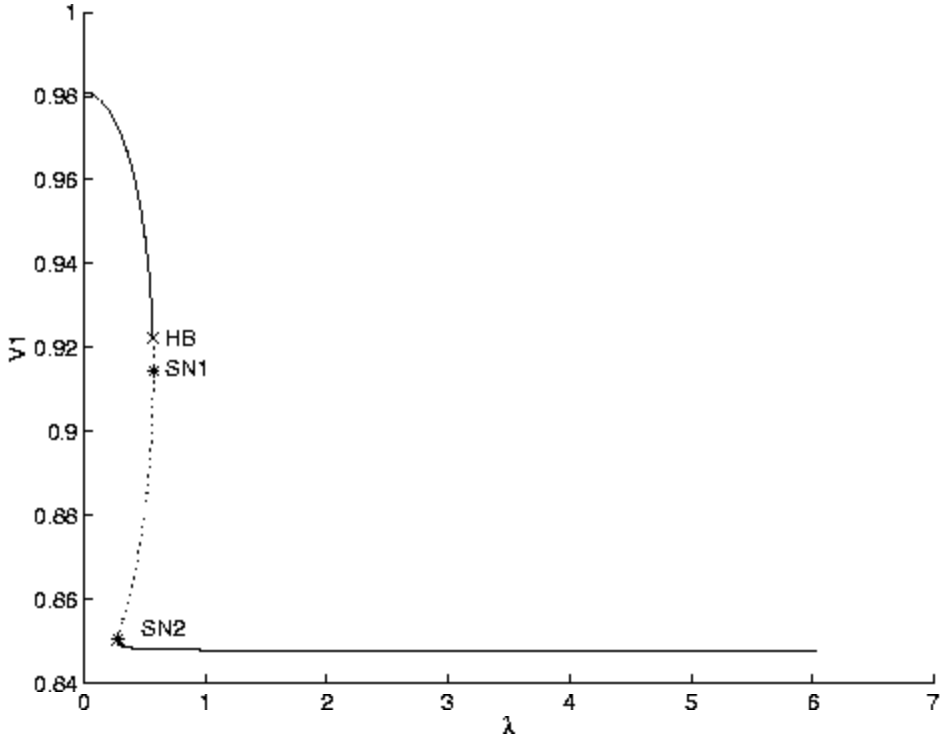

Figure 4.5: Bifurcations diagram of V_1 for fifth order model. The s.c.p.s are represented with a continuous line, whereas the u.c.p.s are depicted with a dotted line.

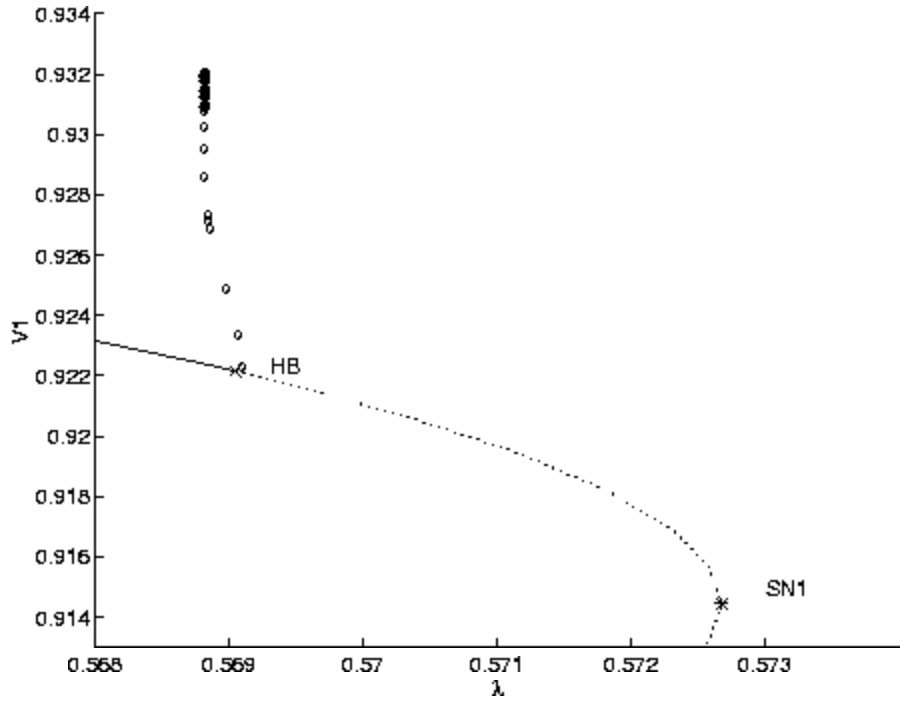

Figure 4.6: Enlargement of the bifurcations diagram of Figure 4.5. Stable and unstable limit cycles are depicted using solid and open circles, respectively.

a subcritical Hopf bifurcation at $k_H = 0.569044$ of an approximate period of 12.6 seconds. The subcritical Hopf occurs just before the first saddle-node in the loading process; this behavior has been reported for other system models [21, 22] as well. The limit cycles associated with the Hopf bifurcation are depicted in Figure 4.5.

Figure 4.7 shows the total load power P versus input voltage V_1 for the system, i.e., the system PV curve. Observe that the Hopf bifurcation (HB) occurs before the nose of the curve or maximum loading point, as shown in Figure 4.8. Also, this maximum loading point does not correspond exactly

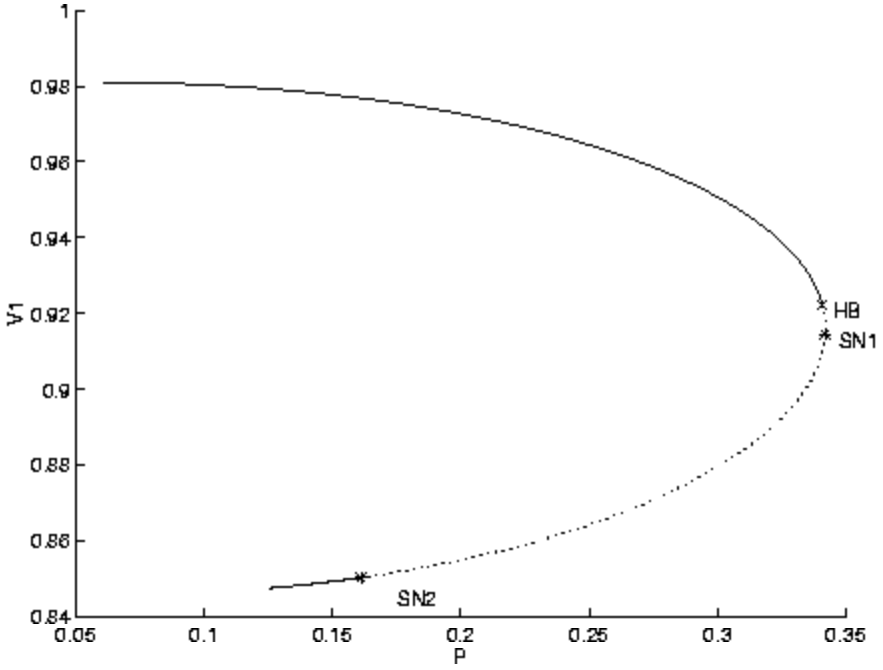

Figure 4.7: PV curve of V_1 for fifth order model. The s.e.p. are represented with a continuous line, whereas the u.e.p. are depicted with a dotted line.

to the first saddle-node bifurcation (SN1). This is expected from the typical relationship between the electro-magnetic torque and the mechanical torque depicted in Figure 4.3. These two points generally coincide when simplified load models are used [9]. The second saddle-node bifurcation (SN2) indicates that stable equilibrium points exist on the lower portion of the curve; this bifurcation is of no practical interest due to the rather low system voltages. A more detailed analysis of induction motor operation on the lower side of the PV curve can be found in [12]. The limit cycles associated to the subcritical Hopf are also depicted in the PV curve of Figure 4.8.

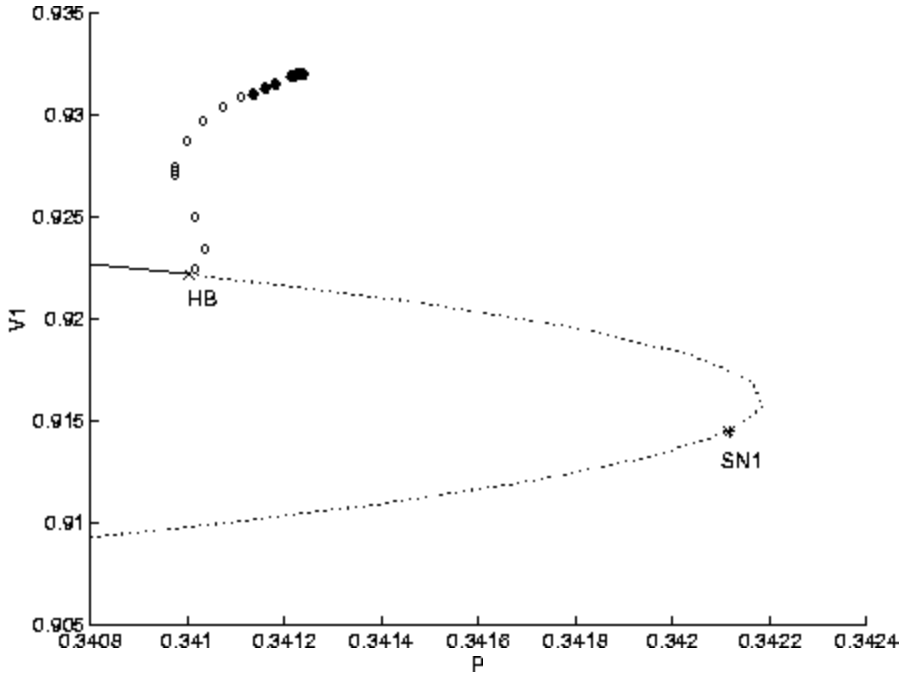

Figure 4.8: Enlargement of PV curve of Figure 4.5. Stable and unstable limit cycles are depicted using solid and open circles, respectively.

Tests with several system models and various parameter values were also carried out to determine their effect on the bifurcation points. For the first and third order models of the induction motor, only the two saddle-node bifurcations were detected. In order to determine the effect of the interaction between the induction motor and the ULTC, the model was modified so that it was composed of only the induction motor, supplied from an equivalent voltage source; in this case only the two saddle-node bifurcations were detected in this case. The values of the different impedances used to represent the static load $G + jB$ and the Thevenin impedance X_{th} were varied, observing that the presence and location of the Hopf bifurcation was a function of the value of X_{th}, and to a lesser extent, G and B. Reducing or increasing the value of X_{th} eliminated the Hopf; a Hopf bifurcation first appears for $X_{th} = 0.074$ for which the distance between the Hopf and the first saddle-node is the greatest. This Hopf moves toward the saddle-node as X_{th} increases and disappears again at $X_{th} = 0.6$. Although changing G and B have similar effects on the Hopf bifurcation, larger value changes are required to obtain similar results as when changing X_{th}.

Due to the algebraic equations introduced with the impedance load, transmission line and the generator, some difficulties arose in the implementation of the system. When using the fifth order induction motor, a closed form expressions describing the system was found in the form of equation (2.4); the software package Maple [42] was used for this purpose. For the first and third order induction motor models, no closed form expression for the algebraic variables could be determined due to their nonlinear complexity; therefore, a numerical non-linear algorithm was used in Matlab.

4.3 Detailed Transmission Line and Load Model

The system considered in Section 4.2 was extended to model the impedance load and the transmission system using differential equations. This allowed for the examination of the interaction of the transmission line and the fifth order induction motor model, and eliminated nonlinear algebraic constraints associated with the transmission line.

As discussed in Chapter 3, a reference frame transformation was applied to the impedance load and the transmission line, and the generator was modeled as a constant voltage source. Since the transmission line and inductive load current (or flux) are now states of the system model, the use of algebraic equations to describe the power flow is not required. The d-axis and q-axis inductances for the transmission line and impedance load were selected to match the steady-state parameters given in Table 4.2.

The following differential equations were used to model the voltage balance from the generator to the load:

$$\begin{aligned} L_{ln}\frac{di_{ln_q}}{dt} &= v_{t_q} - R_{ln}i_{ln_q} - \omega L_{ln}i_{ln_d} - \frac{v_{2_q}}{a} \\ L_{ln}\frac{di_{ln_d}}{dt} &= v_{t_d} - R_{ln}i_{ln_d} + \omega L_{ln}i_{ln_q} - \frac{v_{2_d}}{a} \end{aligned} \tag{4.7}$$

where the subscript ln represents transmission line parameters, v_t is the generator terminal voltage, v_2 is the load bus voltage, and a represents the ULTC tap ratio.

The voltage was defined in terms of the resistance portion of the impedance load. Therefore, the following linear algebraic equations were incorporated in the model:

$$
\begin{aligned}
v_{2_q} &= \left[\frac{i_{ln_q}}{a} - (i_{qs} + i_{load_q})\right] R_{shunt} \\
v_{2_d} &= \left[\frac{i_{ln_d}}{a} - (i_{ds} + i_{load_d})\right] R_{shunt}
\end{aligned} \tag{4.8}
$$

Subscripts used are defined as follows: the subscript s denotes induction motor parameters; *load* corresponds to the inductive portion of the impedance load; v_2 is the voltage at the load bus; ln represents transmission line variables. R_{shunt} is the resistive portion of the impedance load. Because equations (4.8) are linear, they can be directly substituted into equation (4.7).

Equations (3.40), (3.41), (3.45), (3.61), (4.6), (4.7), and (4.8) were then simulated in AUTO97 and Matlab in order to detect bifurcations for the system of Figure 4.2 and Table 4.2. From the simulations, bifurcations diagrams were obtained. In this analysis, only the fifth order induction motor model was used and the ULTC transformer was not removed from the model. Reduced order load models were not considered, since the motivation to include detailed transmission line models was to investigate their appropriateness when examining bifurcations due to induction motors loads; by reducing the order of the induction motor model, the interaction between the transmission system and the induction motor would be effectively removed.

Figures 4.9 depicts the eigenvalues for the range of loading considered in Section 4.2. This figure shows the eigenvalues positioned close to the imaginary axis, however there exists some other eigenvalues of no interest located far from the imaginary axis; there is a pair of purely complex eigenvalues fixed on the imaginary axis. The magnitude of these two eigenvalues, i.e., 377, matches the fundamental radian frequency. The significance of these

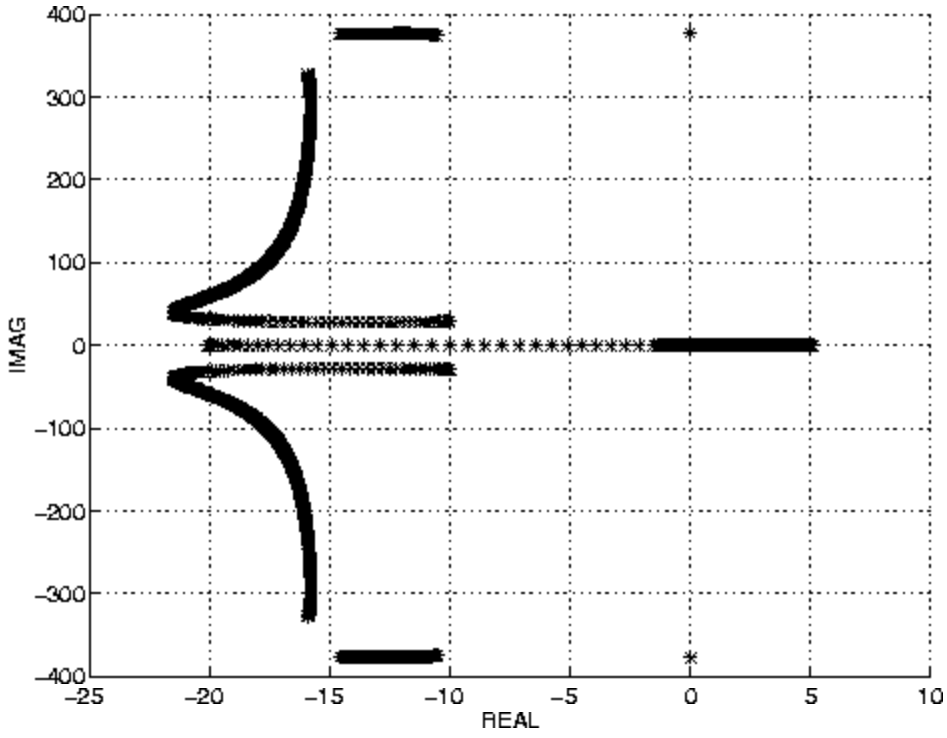

Figure 4.9: Eigenvalues of Detailed Transmission Line and Load Model

eigenvalues is explained below.

The absolute value of the eigenvectors associated with the two imaginary eigenvalues at the initial system loading are shown in Table 4.3. The eigenvectors clearly indicates that the two eigenvalues fixed on the imaginary axis are largely a function of the transmission line q and d-axis current. The initial model did not include the line resistance, i.e., $R_{tr} = 0$. From Chapter 3, it is clear that a system with a source connect in a closed loop composed of strictly inductive elements has eigenvalues fixed on the imaginary axis. Therefore, to remove the pair of eigenvalues fixed on the imaginary axis, a very small line resistance was incorporated into the model; a complete analysis was performed on this model showing that the small resistance did not have an effect on the original system bifurcations. As discussed later, this indicates that the use of lossless transmission line models, when modeling the transmission system with algebraic equations, is acceptable to reduce complexity, but should not be used with more detailed models.

Figures 4.10 through 4.12 depict the equilibrium points (stable and unstable) and bifurcations for the system, as the load varies with changes in the mechanical torque parameter λ. In Figure 4.12, two saddle-node bifurcations at $\lambda_{SN_1} = 0.572672$ and $\lambda_{SN_2} = 0.281250$ are depicted, together with a Hopf bifurcation at $\lambda_H = 5.567003$ of an approximate period of 8.2 seconds. The presence of Hopf bifurcation is clearly illustrated in Figure 4.13 with an enlargement of the eigenvalues of Figure 4.9 focussed at the origin.

The use of differential equations to model the transmission line and impedance load created numerical problems with AUTO97. Due to the size of the problem, the program could not properly analyze the limit cycles as-

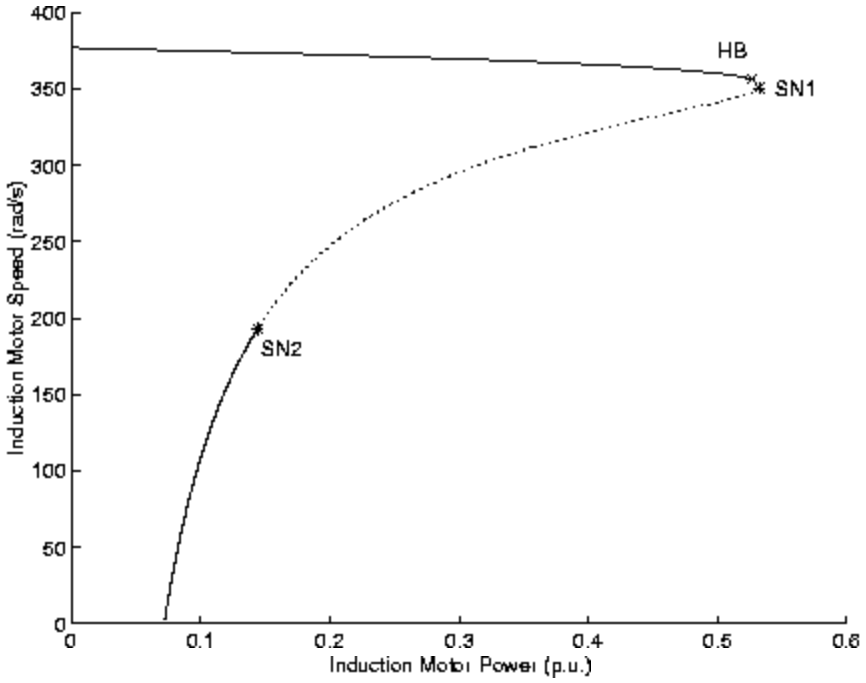

Figure 4.10: Bifurcations diagram of ω_r. The s.c.p. are represented with a continuous line, whereas the u.c.p. are depicted with a dotted line.

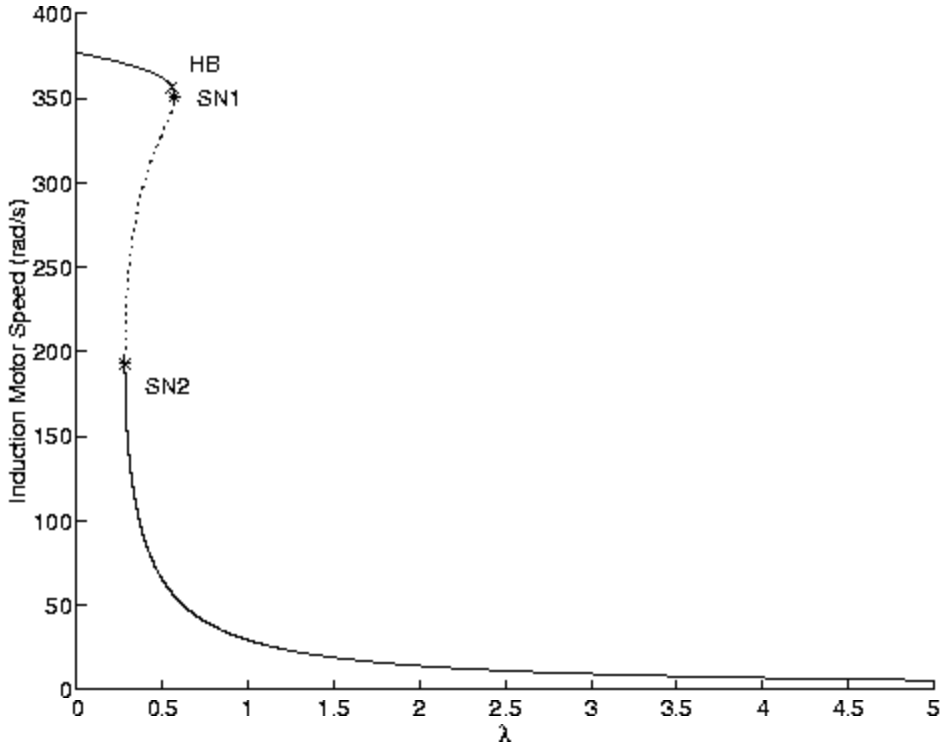

Figure 4.11: Bifurcations diagram of ω_r vs induction motor speed.

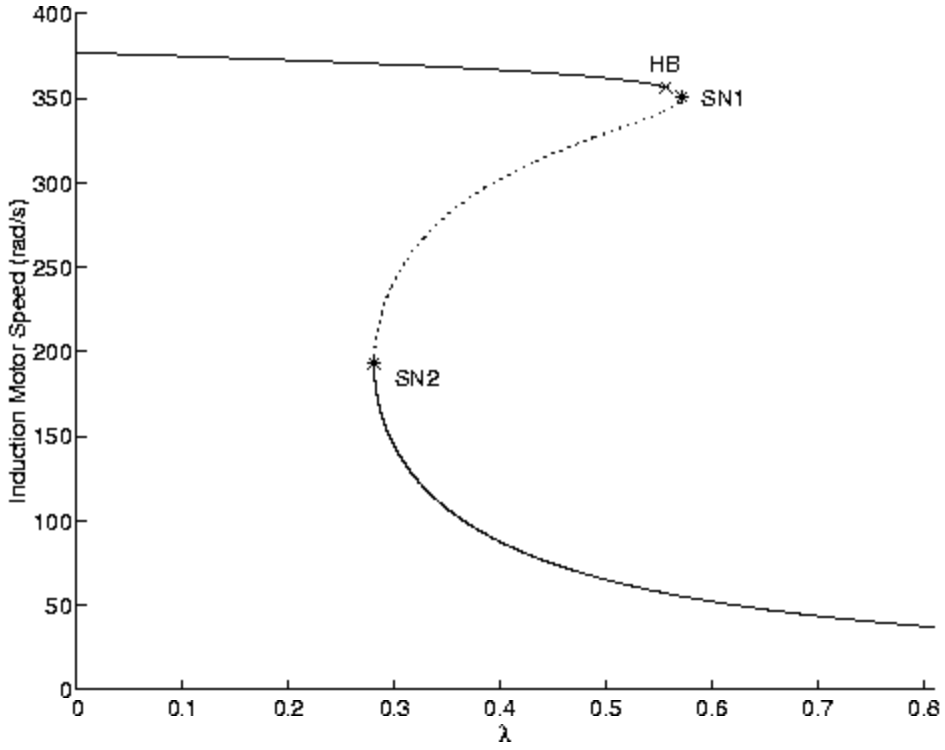

Figure 4.12: Enlargement of the bifurcations diagram of Figure 4.11.

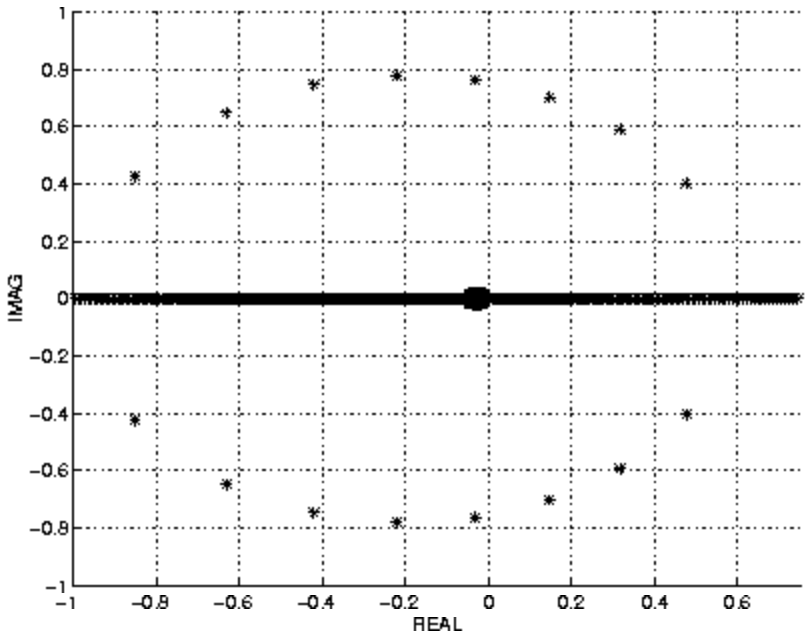

Figure 4.13: Enlargement of the eigenvalue diagram of Figure 4.9.

Table 4.3: Eigenvectors for System at Initial Loading Conditions

Parameter	EV-1
λ_{qs}	1.6228e-10
λ_{ds}	1.6317e-10
λ_{qr}	1.0149e-11
λ_{dr}	1.0093e-11
ω_r	3.5110e-10
I_{ind_q}	4.9057e-01
I_{ind_d}	4.9057e-01
I_{ln_q}	5.0926e-01
I_{ln_d}	5.0926e-01
a	2.4972e-14

sociated with the Hopf bifurcation.

4.4 Detailed System Model

The final analysis incorporated a detailed model for the entire system, including the synchronous generator; the generator model used is described in Section 3.3. In the analysis, typical synchronous machine parameters described in [38] were used, and are listed in Table 4.4.

To allow for an accurate comparison between the previous two models, the droop of the generator governor was set to zero. Furthermore, the AVR was set to maintain the same voltage magnitude as with other models. Due to the nature of the machine model, the composition of the generator terminal

Table 4.4: Synchronous Generator Parameters

Variables	Value
V_{kq1}	0.0000 pu
V_{kq2}	0.0000 pu
k_d	0.0000 pu
T_a	2.0000 pu
H	2.3700 pu
T_{b2}	1.0000 pu
ω_e	377 pu
R_s	0.000100 pu
R_{kq2}	0.054000 pu
R_{fd}	0.000742 pu
R_{kd}	0.001096 pu
X_{ls}	0.090000 pu
X_{fd}	0.015000 pu
X_{kd}	1.605000 pu
X_{kq2}	1.526000 pu
X_q	1.6400 pu
X_d	1.7000 pu
X_{mq}	0.028378 pu
X_{md}	0.028378 pu

voltage is different than the other model. In the first two models, the d-axis voltage was set to zero and the q-axis voltage was set to unity. Using the detailed generator model, this is not possible, as the d-axis voltage is a function of the d-axis current. Although the composition of the total voltage magnitude was fundamentally composed of the q-axis voltage, the difference in the models should be noted. Furthermore, a ground shunted resistance was added at the generator bus. This was done to be able to mathematically define the voltage at the terminal of the generator bus. The addition of the resistor also reduced the complexity of the differential equations, as it serves to isolate the transmission line current and the generator current.

Equations (3.61), (3.41), (3.40), (3.45), (3.46)-(3.54), (3.58), (3.59), (4.6), (4.7) and (4.8) were simulated in Matlab in order to obtain the bifurcation diagrams for the test system of Figure 4.2 and Tables 4.2 and 4.4.

Figure 4.14 depicts the equilibrium points (stable and unstable) and bifurcations for the complete system model, as the load varies with changes in the mechanical torque parameter λ. Two saddle-node bifurcations at $\lambda_{SN_1} = 0.572660$ and $\lambda_{SN_2} = 0.281250$ are present in the system, with a Hopf bifurcation at $\lambda_H = 0.555149$. Again, the Hopf bifurcation occurs just before the first saddle-node in the loading process.

Because of the number of states in the complete model, AUTO97 was not able to perform the analyses. Matlab was used to determine initial starting points with over six digits of accuracy but, AUTO97 still was not able to converge. Recompiling AUTO97 to increase the number of parameters it can perform bifurcation analyses for did not improve the program's capability, therefore, Matlab routines were used to calculate the equilibrium points and

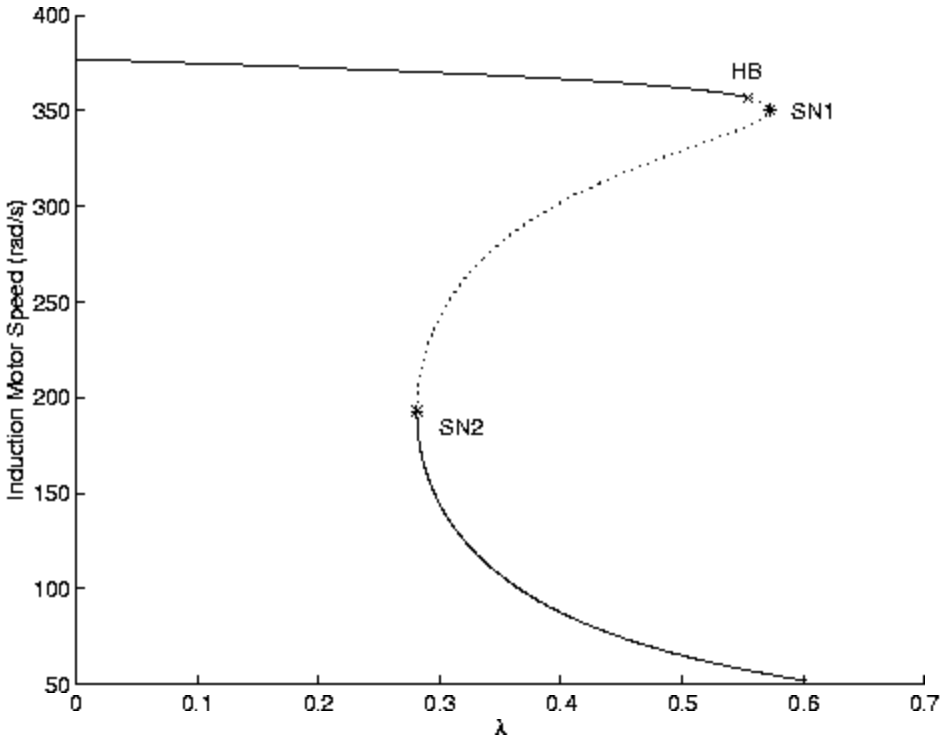

Figure 4.14: Bifurcations diagram of ω_r for complete system model. The s.c.p.s are represented with a continuous line, whereas the u.c.p.s are depicted with a dotted line.

eigenvalues.

4.5 Summary of Results

In this Chapter, several models for the same power system were used. The most detailed system model included a complete description of the system from the generator to the load. The least detailed model, used a third order induction motor model and several nonlinear algebraic equations for modeling the transmission system and the supply system. For each model, parameters were determined such that the models had equal steady state values for equivalent loading levels. A minor exception to this occurred with the voltages of the detailed generator model, described in Section 4.4, because of the nature of the synchronous machine model, as compared to a Thevenin equivalent.

Table 4.5 illustrates the bifurcations that were encountered for the different models. For the first and third order models of the induction motor, only the two saddle-node bifurcations were detected. When the ULTC transformer was removed from the model, again only the two saddle-node bifurcations were detected.

The results shown in Table 4.5 indicate that the first order model is an acceptable approximation to the full aggregated induction motor dynamics, when the the objective of the analysis is mostly interested in the location of saddle-node and other bifurcations. For analysis of higher order dynamics, such as Hopf bifurcations, more detailed models are required, which is expected from previous results [21, 22].

Table 4.5: Eigenvalues for Saddle Node, SN, and Hopf Bifurcations, HB, for Different Models

System Model	SN_1	SN_2	HB
Detailed Induction Motor and ULTC Model (Sec. 4.2)			
• Fifth Order Motor Model with ULTC	0.572672	0.281250	0.569044
• Fifth Order Motor Model without ULTC	0.512377	0.228047	No Hopf
• Third Order Motor Model with ULTC	0.572672	0.281250	No Hopf
• First Order Motor Model with ULTC	0.572672	0.281250	No Hopf
Detailed Transmission Line and Load Model (Sec. 4.3)	0.572672	0.281250	0.5567003
Detailed System Model (Sec. 4.4)	0.572660	0.281250	0.555149

The *Detailed Induction Motor and ULTC Model* section of Table 4.5 indicate that system components, such as the ULTC transformer, play a critical role in the occurrence of Hopf bifurcations and indicates that some elements in a power system cannot be evaluated independently, as their interaction may significantly affect the dynamic response. But the remaining sections, showing results when detailed models of the transmission system and generator have been included, indicate these component do no have a large effect on the occurrence of bifurcations in this case. The detailed models do have a minor effect of the location of the bifurcations and also on the initial period of the Hopf bifurcation, as shown in Table 4.6. This suggests that the need to model transmission systems using differential equations in bifurcations studies may not be required for the detection of bifurcations. However, more studies are required before definite conclusions can be drawn.

Table 4.6: Initial Periods of Hopf Bifurcations for Different Models

System Model	Period (seconds)
Detailed Induction Motor and ULTC Model (Sec. 4.2)	
• Fifth Order Motor Model with ULTC	12.6
Detailed Transmission Line and Load Model (Sec. 4.3)	8.2
Detailed System Model (Sec. 4.4)	4.3

4.6 Notes on AUTO97

Although AUTO97 was found in general to be a reliable tool for the work presented in this thesis, it should be noted that:

1. AUTO97 required very close initial conditions to be able to converge to an initial equilibrium point; hence, other packages were used to determine good initial conditions. From the initial point, the program uses a continuation method to find other equilibrium points, and a direct method to find the bifurcation points when these are detected; AUTO97 was very robust in tracing the solution set in all directions.

2. AUTO97's output capability is initially limited to five states. A minor modification in the output code was implemented to increase this value to meet greater requirements.

3. Algebraic constraints were difficult to incorporate in AUTO97 , and this became very apparent in the first and third order induction motor models. The algebraic constraints became a limiting factor in the analysis, as the program assumes that the system model is made up of

only differential equations. Thus, the vector equations used in AUTO97 were rewritten as follows:

$$\begin{aligned} y &= h(x, \lambda) \\ \dot{x} &= f(x, y, \lambda) \end{aligned}$$

so that the algebraic constraints could be directly evaluated. This required the use of other software packages to find a closed expression for the fifth order model. The closed form expressions for the first and third order models were not pursued because of their complexity; Matlab was used to study the bifurcations in these cases.

Chapter 5

Eliminating Algebraic Constraints

In the current literature of stability analysis, generators and/or the loads are modeled using differential equations, but the transmission system is generally modeled using algebraic variables. In [10], the use of dynamic transmission circuit models are introduced, with a simple single machine example. In Chapter 4, differential equations to model the transmission system were introduced into the model. Hence, for completeness, the introduction of dynamic transmission system modeling is extended to a multi-bus system to discuss its use in traditional system models and related studies, such as power flows and stability analysis (transient and steady state).

In this Chapter, first the traditional system model is reviewed. The proposed dynamic model is then presented, using a generalized format so that it can be applied to any load flow and stability problem. A comparison of the algorithms is then done using a sample system.

5.1 Traditional System Model

In power system analysis, the time frame associated with the dynamics being considered can vary dramatically. The time response of exciter and some controllers are fast, where as mechanical devices such as boiler controllers have very slow transients. Most components of the power system can be described dynamically, but in most models some dynamics are not included. For example, when analyzing the switching of power electronic devices, which have very fast dynamics, the slow dynamics of transformer taps and boilers are ignored. When analyzing components with fast dynamics the analysis is done for only a short period of time, usually measured in milliseconds. When considering components with slower dynamics, the dynamics of faster components are usually ignored. In most studies, components with dynamic responses of similar time constants are analyzed together.

When the dynamics of a component is ignored, the differential equation used to model that component is transformed into an algebraic constraint. For example, considering the induction motor stator flux linkage transients (Section 3.2.3):

$$\begin{aligned} \dot{\psi}_{ds} &= \omega_b(v_{ds} - R_s i_{ds} - \frac{\omega_b}{\omega_e}\psi_{qs}) \\ \dot{\psi}_{qs} &= \omega_b(v_{qs} - R_s i_{qs} + \frac{\omega_b}{\omega_e}\psi_{ds}) \end{aligned} \tag{5.1}$$

Ignoring the stator flux linkage transients, i.e., $\dot{\psi}_{qs} = \dot{\psi}_{ds} = 0$, transform equations (5.1) into the following algebraic constraints:

$$0 = \omega_b(v_{ds} - R_s i_{ds} - \frac{\omega_b}{\omega_e}\psi_{qs}) \tag{5.2}$$
$$0 = \omega_b(v_{qs} - R_s i_{qs} + \frac{\omega_b}{\omega_e}\psi_{ds})$$

If all the dynamics of the power system are considered, then equations (2.1) and (2.2) can be written as:

$$\begin{bmatrix} \dot{x} = f(x, y, \lambda) \\ 0 = g(x, y, \lambda) \end{bmatrix} \quad \Rightarrow \quad \dot{x} = f(x, \lambda) \tag{5.3}$$

Where $g(x, y, \lambda)$ is excluded since no algebraic constraints have been introduced, and the linear relationship between currents and flux are assumed to have been incorporated into the dynamic equations.

In stability analysis, models are generally composed of differential-algebraic equations which can be written in the form of equations (2.1) and (2.2). Typically, the dynamics associated with transmission lines are ignored, since the time response of the transmission line is very fast as compared to the other system components. The transmission system is modeled by introducing algebraic constraints which typically correspond to the classical power flow model. The algebraic constraints generated by removing the transients associated with the transmission lines are generally rather nonlinear. This leads, for certain loading conditions, to numerical difficulties, as the constraints may become singular, rendering the model unsolvable. The proposed system model incorporates the dynamics associated with the transmission line and impedance loads, *without the need for additional data.*

5.2 Proposed System Model

As discussed in Chapter 2, the typical form of the system equations for stability studies is:

$$\dot{x} = f(x, y, \lambda) \tag{5.4}$$

$$0 = g(x, y, \lambda) \tag{5.5}$$

Most power system stability analyses make the assumption that equation (5.5) is non-singular and, therefore, can be directly or indirectly substituted into (5.4). Intuitively this approach does not seem acceptable in all cases. For example, if the transmission system is approaching the traditional maximum power transfer limit, the interaction between the dynamically modeled load and/or generators with the transmission system may play a significant role in resulting bifurcation problems.

Although, the use of differential equations to model the transmission line in Chapter 4 did not remove all the algebraic equations, it did remove all the nonlinear algebraic equations. The only remaining algebraic equations are linear constraints.

The generalized algorithm for using differential equations to model a transmission system is an extension of the model presented in Section 3.5. The transmission system is modeled in the dq0 reference frame based on the angular speed of the system slack generator.

Figure 5.1 illustrates a generic single line diagram for a branch between two nodes; the diagrams for the d and q axis are the same. ULTC transformers have been placed at each bus to improve the portability of the algorithm.

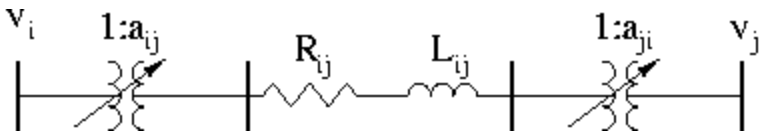

Figure 5.1: Transmission line single line diagram

If no transformer is present, then the tap setting is fixed at unity and the differential equation used to model the transformer is excluded. Kirchhoff's voltage law for this circuit gives:

$$a_{ij}v_{q_i} - \frac{v_{q_j}}{a_{ji}} = Ri_q + \omega X_{ij}i_q + X_{ij}\frac{d}{dt}i_q \tag{5.6}$$

$$a_{ij}v_{d_i} - \frac{v_{d_j}}{a_{ji}} = Ri_d - \omega X_{ij}i_d + X_{ij}\frac{d}{dt}i_d \tag{5.7}$$

Equations (5.6) and (5.7) are written in the standard format of equation (5.4) as follows:

$$\dot{i}_q = \frac{1}{X_{ij}}(a_{ij}v_{q_i} - \frac{v_{q_j}}{a_{ji}} - Ri_q - \omega X_{ij}i_q) \tag{5.8}$$

$$\dot{i}_d = \frac{1}{X_{ij}}(a_{ij}v_{d_i} - \frac{v_{d_j}}{a_{ji}} - Ri_d + \omega X_{ij}i_d) \tag{5.9}$$

In order to numerically isolate variables at buses, shunt resistors are used, this prevents complicated expressions from arising due to combining equations from one transmission line into another or with a load. Determining the bus voltages is also simplified using the isolating resistor. In some cases, shunt resistors will be present due to an existing load; if there is no load resistance present, a resistance of 10^6 pu is used, allowing for the numerical isolation without having a significant impact on the circuit. A shunt resistor

is also used at generator buses to define the voltage for the automatic voltage regulator. The EPRI simulation package, EMTP, uses a similar numerical method in defining voltages at generator buses [43].

Including equations (5.8) and (5.9) into the system model increases the number of differential equations in the model by two (d and q axis current) for each line, but also decreases the number of existing non-linear algebraic equations by two.

To further eliminate non-linear algebraic equations, the system generators must also be modeled using differential equations. In typical stability studies, generator models include dynamic behavior for the stator d and q axis current, the field current, the field voltage, automatic voltage regulator and governor models. Non-slack generators are modeled without a governor as the mechanical power is fixed for these machines, since they represent constant power-voltage machines; the behavior of the non-slack bus generators is discussed in greater detail in the following section. A detailed generator model is given by equations (3.46)-(3.59) in Chapter 3.

Shunt capacitance can be included into the transmission line model by adding capacitors to the terminals as illustrated in Figure 5.2. The corresponding $qd0$ transformation for capacitors allows for their easy integration into the model.

5.2.1 Non-Slack Bus Generators

One significant modification to the system model presented in Chapters 3 is the addition of the non-slack generators. In order to incorporate the generator into the present model, the behavior of the non-slack machines is

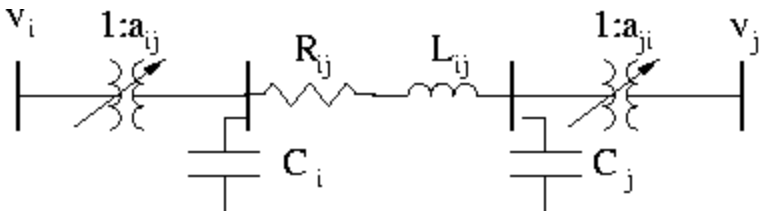

Figure 5.2: Transmission line single line diagram with capacitance

reviewed. In steady state, the frequency of each of the generators must be equal to the frequency of the system and is controlled by the slack bus. If one of the generator's frequency is greater than the system frequency, the mechanical power input of this generator is greater than its electrical power output. As the generator increases in speed, the angle between this generator's d-q reference will increase relative to the system's d-q reference. The opposite applies when the non-slack generator's frequency is less than the system frequency. In balanced steady state operation, the rate of increase of the relative angles of the reference frames is zero, but the value of the angle may not be zero. That is:

$$\dot{\delta_{21}} = 0 \tag{5.10}$$
$$\delta_{21} = c$$

where the subscripts 12 are used to represent the angle δ between the two reference frames denoted as 1 and 2, and c is a constant.

Therefore, it is important that transformations are included to transform parameters from the system d-q axis to non-slack generators d-q axis frame. The standard transformation between reference frames is [33] :

$$f''_{qd} = {}' K'' f'_{qd} \tag{5.11}$$

$${}'K'' = \begin{bmatrix} cos(\delta_{21}) & -sin(\delta_{21}) \\ sin(\delta_{21}) & cos(\delta_{21}) \end{bmatrix} \tag{5.12}$$

$$\delta_{21} = \delta_2 - \delta_1 \tag{5.13}$$

where f represents any of the electrical variables (current, voltage, flux linkage). Because of its structure, equation (5.11) is invertible for any value of δ_{21}, as the determinant of equation (5.12) is always equal to one.

The transformation presented above is then used to transform voltages and currents from non-slack generator dq0 reference frames to the transmission system's dq0 reference frame. To define the angle δ_{21}, the rotor speed of the non-slack generator is required:

$$\dot{\omega}_r = \frac{\omega_e}{2H}(T_e - T_m) \tag{5.14}$$

where T_e and T_m are the electro-magnetic torque and mechanical torque, respectively; ω_e is the base angular frequency; and ω_r is the angular speed of the rotor. As described above, the behavior of the angle δ_{21} is a function of the difference between the non-slack generator speed ω_r and the angular frequency of the system ω_1, i.e.:

$$\dot{\delta}_{21} = \omega_r - \omega_1 \tag{5.15}$$

5.3 Numerical Example

Numerical simulations were performed on a three bus, two generator power system illustrated in Figure 5.1. The generator located at BUS 1 acts as the system slack bus, and the generator at BUS 2 is a constant voltage-power controlled bus. The parameters for each of the generators are given in Table 5.1. An impedance load is connect to each of the buses, with the greatest load occurring at BUS 3. The parameters for the impedance loads are given an Table 5.2, and the parameters for the transmission system are given in Table 5.3.

5.3.1 System Model

For clarity, the entire system model is described. The model for the synchronous machine is a reduced order model based on the full model developed in Chapter 3. The dynamic nature of the stator flux are given by:

$$\dot{\psi}_{qs} = \omega_e \left(v_{qs} + R_s i_{qs} - \frac{\omega_r}{\omega_e} \psi_{ds} \right) \tag{5.16}$$

$$\dot{\psi}_{ds} = \omega_e \left(v_{ds} + R_s i_{ds} + \frac{\omega_r}{\omega_e} \psi_{qs} \right) \tag{5.17}$$

where the stator s and rotor r variables v, i, and ψ stand for the dq voltages, currents, and flux linkages, respectively. The rotor speed is represented by ω_r, and $\omega_e = 2\pi 60$ is the synchronous speed. The stator winding resistance is R_s. The damper windings of the machine were not included in the model since the purpose was not to model generator dynamics in great detail, but these could be added if required.

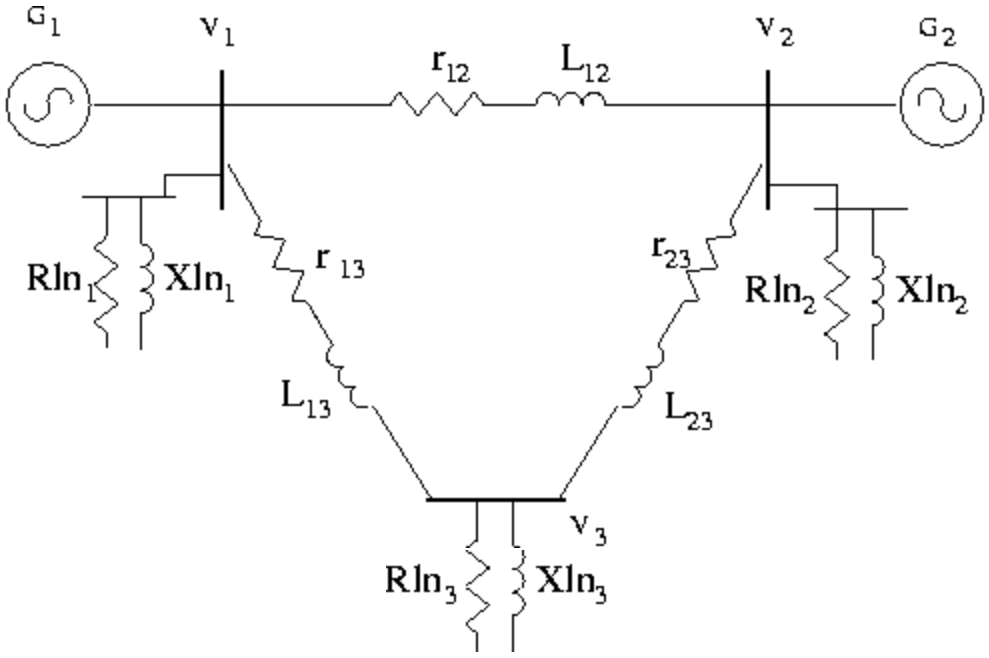

Figure 5.3: Transmission Line Single Line Diagram

Table 5.1: Synchronous Generator Parameters

Variables	Generator 1	Generator 2
H	2.3700 s	2.8000 s
ω_{base}	377 rad/s	377 rad/s
R_s	0.0014 pu	0.0014 pu
R_{fd}	0.0079 pu	0.0706 pu
X_{ls}	0.0535 pu	0.0535 pu
X_{fd}	0.0706 pu	0.0706 pu
X_q	0.0461 pu	0.0461 pu
X_d	0.0695 pu	0.0695 pu

Table 5.2: Impedance Load Parameters

Bus Number	R	L
Bus 1	7.0727 pu	0.0281 s
Bus 2	5.4080 pu	0.0191 s
Bus 3	1.2252 pu	0.0054 s

Table 5.3: Transmission Line Parameters

Sending Bus	Receiving Bus	R_{line}	L_{line}
Bus 1	Bus 2	0.0100 pu	1.5915e-04 s
Bus 1	Bus 3	0.0800 pu	6.3662e-04 s
Bus 2	Bus 3	0.0600 pu	4.7746e-04 s

The dynamic behavior of the flux generated by the field winding is given by equation (5.18). The automatic voltage regulator is described by equation (5.19) and (5.20).

$$\dot{\psi}_{fd} = \omega_b(v_{fd} - R_{fd}i_{fd}) \tag{5.18}$$

$$\dot{v}_{fd} = \frac{1}{T_a}(V_{ref} - V_t) \tag{5.19}$$

$$V_t = \sqrt{v_{qs}^2 + v_{ds}^2} \tag{5.20}$$

where T_a is the time constant of the AVR, V_{ref} is a reference signal, i_{fd} is the field current, v_{fd} is the field voltage, and V_t is the generator terminal voltage.

The governor and speed of the slack generator are defined by equations (3.58) and (3.59). The relationship between the machine's fluxes and currents are described by equations (3.51). All parameters in equations (5.16)-(5.19) are in the dq0 reference frame of the generator they are describing.

Using equations (3.69), the transmission lines are modeled as follows:

$$\dot{i}_{q12} = \frac{1}{L_{12}}(v_{q1} - R_{12}i_{q12} - \omega L_{12}i_{d12} - v_{q2}) \quad (5.21)$$
$$\dot{i}_{d12} = \frac{1}{L_{12}}(v_{d1} - R_{12}i_{d12} + \omega L_{12}i_{q12} - v_{d2})$$

$$\dot{i}_{q13} = \frac{1}{L_{13}}(v_{q1} - R_{13}i_{q13} - \omega L_{13}i_{d13} - v_{q3}) \quad (5.22)$$
$$\dot{i}_{d13} = \frac{1}{L_{13}}(v_{d1} - R_{13}i_{d13} + \omega L_{13}i_{q13} - v_{d3})$$

$$\dot{i}_{q23} = \frac{1}{L_{23}}(v_{q2} - R_{23}i_{q23} - \omega L_{23}i_{d23} - v_{q3}) \quad (5.23)$$
$$\dot{i}_{d23} = \frac{1}{L_{23}}(v_{d2} - R_{23}i_{d23} + \omega L_{23}i_{q23} - v_{d3})$$

where L is the impedance of the line in the dq0 reference frame; the transmission line currents and the bus voltages for the d and q axes are given as i and v, respectively, with their subscripts identifying their location; and ω is the dq0 transformation reference frame speed. All parameters in equations (5.21)-(5.23) are in the transmission system reference frame, defined by ω.

The inductive component of the impedance loads are modeled based on the model presented in equation (3.30) in Section 3.1.2; the equations for the inductive components are then:

$$\begin{aligned} \dot{i}_{load_q1} &= \frac{v_{q1}}{L_{load1}} - \omega i_{load_d1} \\ \dot{i}_{load_d1} &= \frac{v_{d1}}{L_{load1}} + \omega i_{load_q1} \end{aligned} \tag{5.24}$$

$$\begin{aligned} \dot{i}_{load_q2} &= \frac{v_{q2}}{L_{load2}} - \omega i_{load_d2} \\ \dot{i}_{load_d2} &= \frac{v_{d2}}{L_{load2}} + \omega i_{load_q2} \end{aligned} \tag{5.25}$$

$$\begin{aligned} \dot{i}_{load_q3} &= \frac{v_{q3}}{L_{load3}} - \omega i_{load_d3} \\ \dot{i}_{load_d3} &= \frac{v_{d3}}{L_{load3}} + \omega i_{load_q3} \end{aligned} \tag{5.26}$$

where the d-axis and q-axis variables include the inductor current, represented by i_{load}, and the voltage at the load bus, represented with the standard notation v. All parameters in equations (5.24)-(5.26) are in the transmission system reference frame.

The voltage at each of the buses are defined simply by applying Kirchhoff's current law and Ohms law at each bus. The current through the shunt resistor must equal the net current flow into the bus, the voltage is then determined by multiplying the net current flow at the bus by the value of the bus shunt resistance. Therefore, the bus voltages are defined using the following linear algebraic equations:

$$
\begin{aligned}
v_{q1} &= (i_{qs1} - i_{q12} - i_{q13} - i_{load_q1})R_{load_1} \qquad (5.27)\\
v_{d1} &= (i_{ds1} - i_{d12} - i_{d13} - i_{load_d1})R_{load_1}
\end{aligned}
$$

$$
\begin{aligned}
v_{q2} &= (i_{qs2} + i_{q12} - i_{q23} - i_{load_q2})R_{load_2} \qquad (5.28)\\
v_{d2} &= (i_{ds2} + i_{d12} - i_{d23} - i_{load_d2})R_{load_2}
\end{aligned}
$$

$$
\begin{aligned}
v_{q3} &= (i_{q13} + i_{q23} - i_{load_q3})R_{load_3} \qquad (5.29)\\
v_{d3} &= (i_{d13} + i_{d23} - i_{load_d3})R_{load_3}
\end{aligned}
$$

where i_{qs} and i_{ds} represents the current from the generators. All parameters in equations (5.27)-(5.29) are in the transmission system reference frame.

The transformation outlined in Section 5.2.1 is then applied to transform the BUS 2 voltages and currents from the system reference frame (governed by the speed of the slack generator) and the reference frame of the generator at BUS 2. These transformations are as follows:

$$
\begin{aligned}
i''_{qs2} &= i'_{qs2}\cos(\delta_{21}) \quad -i'_{ds2}\sin(\delta_{21}) \qquad (5.30)\\
i''_{ds2} &= i'_{ds2}\sin(\delta_{21}) \quad +i'_{ds2}\cos(\delta_{21})
\end{aligned}
$$

$$
\begin{aligned}
v''_{qs2} &= v'_{qs2}\cos(\delta_{21}) \quad -v'_{ds2}\sin(\delta_{21}) \qquad (5.31)\\
v''_{ds2} &= v'_{ds2}\sin(\delta_{21}) \quad +v'_{ds2}\cos(\delta_{21})
\end{aligned}
$$

where the superscripts $'$ and $''$ indicate that the parameter is in the transmission reference frame, or in the BUS 2 generator reference frame, respectively.

The current and voltages from the slack generator (BUS 1 generator) do not require transformations, since the system reference frame is based on the slack bus generator reference frame. Finally, equations (5.14) and (5.15) are used to define the angle δ_{21}, with $\delta_{12} = -\delta_{21}$.

5.3.2 Simulation Results

The twenty-four differential equations used to model the system were incorporated into Matlab based routines to determine the steady-state and time-domain solution of the system.

The steady state results are shown in Table 5.4. To ensure the reliability of the proposed algorithm the solution was also found using a traditional load flow algorithm, which is given in Table 5.5. The percent difference between the results of the two algorithms, shown in the last column of Table 5.5, demonstrates that the algorithms converge with only minor differences to the same solution.

The time domain simulation of the system when a three phase ground fault is applied at BUS 2 is shown in Figures 5.4 through 5.7. The fault was applied for 150 milliseconds before being cleared. Figures 5.4 and 5.6 are the time domain response using the proposed algorithm. Figures 5.5 and 5.7 are the response using the typical transient stability model of the same system. The transient stability model makes the assumption that the frequency of the system does not vary significantly and uses phasors to model the transmission system. The figures indicate that the proposed model can be used to accurately perform transient stability analysis. The additional oscillations of the BUS 2 voltage illustrates the interaction of the transmission

system and load dynamics in the proposed model. This interaction can not occur in the traditional model.

Because the time constants of the proposed model associated with the transmission system are very small, numerical integration is computationally intensive. The use of explicit integration methods, such as the Runge-Kutta was not feasible in this case due to time and memory requirements; implicit methods methods were successfully applied.

5.4 Summary of Results

In this Chapter, a new model is proposed for modeling power systems in bifurcation studies. The model was also shown to be accurate for transient stability studies. The typical transient stability model is a subset of the proposed model, since transient stability models consider dynamics of generators and loads but not dynamics of the transmission system. The "quasi-steady-state" phasor models used in transient stability studies to represent the transmission system has been replaced by dynamic variables. To transform the proposed model to the "quasi-steady-state" phasor model, the dynamics associated with the transmission line are set to zero. The proposed model makes no assumptions about fluctuation in the system frequency, which are ignored in typical transient stability models. The disadvantage of the proposed model is some numerical integration problems due to the large differences in time constants of the different element modes, although implicit integration techniques can be used to partly overcome this problem. However, the proposed model guarantees that the algebraic constraints will remain non-singular.

Table 5.4: Load Flow Results - Dynamic Algorithm

Variable	Value
Bus 1 q-axis Voltage	1.0296 pu
Bus 1 d-axis Voltage	0.0303 pu
Bus 1 Voltage Magnitude	1.0300 pu
Bus 1 Voltage Angle	0°
Bus 2 q-axis Voltage	1.0391 pu
Bus 2 d-axis Voltage	0.0431 pu
Bus 2 Voltage Magnitude	1.0400 pu
Bus 2 Voltage Angle	0.6924°
Generator 2 Machine Angle	1.3592°
Bus 3 q-axis Voltage	0.9539
Bus 3 d-axis Voltage	0.0943
Bus 3 Voltage Magnitude	0.9586
Bus 3 Voltage Angle	3.9612°

Table 5.5: Load Flow Results - Traditional Algorithm

Variable	Value	% diff. to Dynamic Algorithm
Bus 1 Voltage Magnitude	1.0300 pu	0
Bus 1 Voltage Angle	0°	0
Bus 2 Voltage Magnitude	1.0400 pu	0
Bus 2 Voltage Angle	0.6820°	1.5 %
Bus 3 Voltage Magnitude	0.9586	0
Bus 3 Voltage Angle	3.9552°	0.15 %

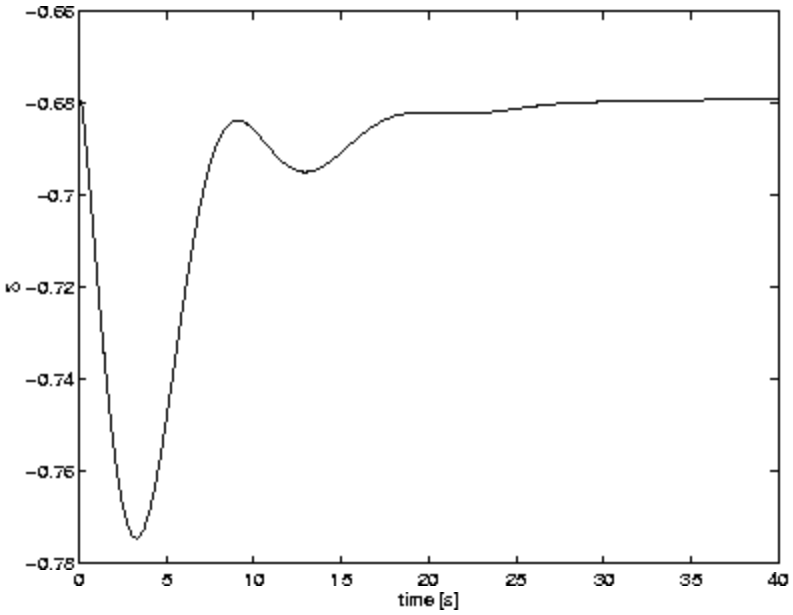

Figure 5.4: Transient response of Generator 2 machine angle δ_{21} with a three phase ground fault applied at Bus 2 at $t = 0.1s$ for 150 milliseconds.

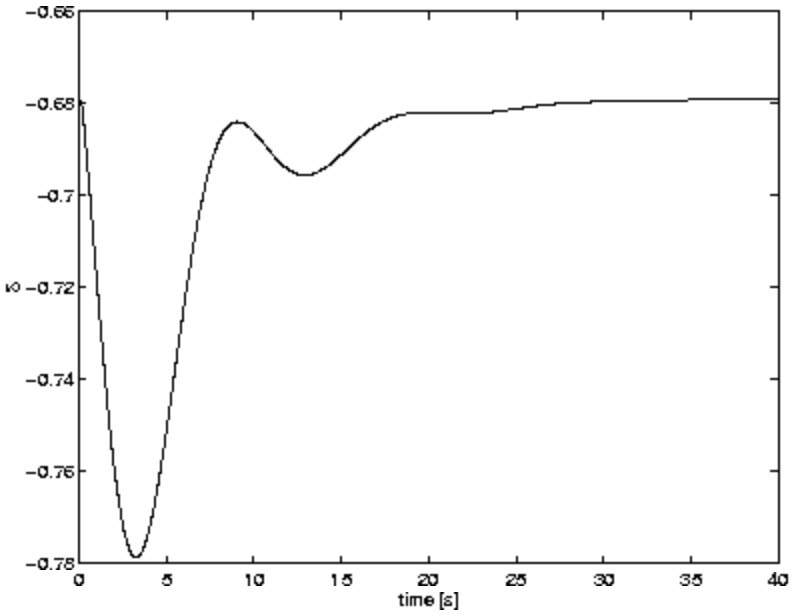

Figure 5.5: Proposed models response of Generator 2 machine angle δ_{21} with a three phase ground fault applied at Bus 2 at $t = 0.1s$ for 150 milliseconds

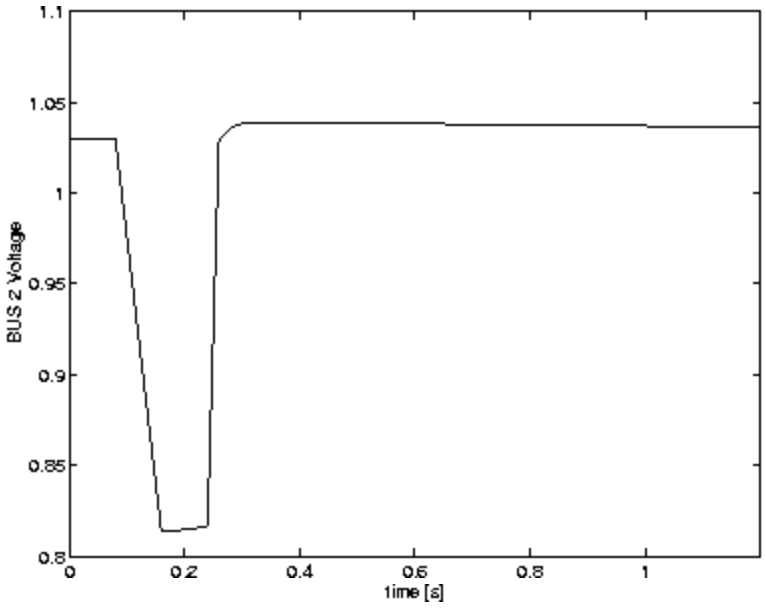

Figure 5.6: Transient response of BUS 2 voltage with a three phase ground fault applied at Bus 2 at $t = 0.1s$ for 150 milliseconds for time period 0 to 1.2 seconds.

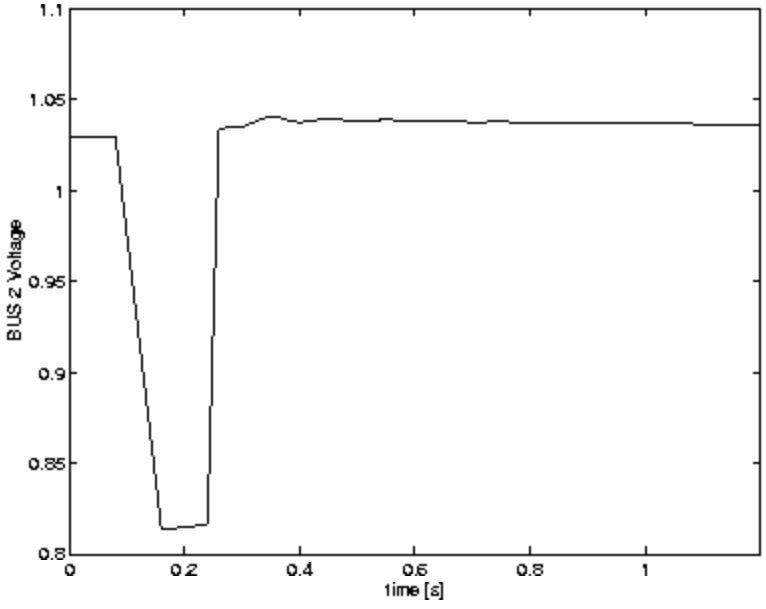

Figure 5.7: Proposed models response of BUS 2 voltage with a three phase ground fault applied at Bus 2 for $t = 0.1s$ for 150 milliseconds for time period 0 to 1.2 seconds.

Chapter 6

Conclusions

This thesis has presented a complete bifurcation study of several different models of an induction motor fed by an ULTC transformer with detailed generator and transmission system models. First order models of induction motors are shown to be adequate for saddle-node bifurcation studies, whereas steady state models are proven to be inadequate for these types of analyses. The results indicate that at least the mechanical dynamics of aggregated loads should be included in voltage collapse studies of power systems, so that reasonable results can be obtained. When oscillatory modes associated with Hopf bifurcations are of interest, high order models must be used.

The complex dynamic behavior observed due to the interaction of an ULTC and an aggregated induction motor load suggested that using more detailed models of the generator, static loads and transmission systems would demonstrate the interactions between the network and its different loads. However, including detailed models of the transmission system and generator did not significantly change the formation of bifurcations. This indicates

that the need to model transmission systems using differential equations in bifurcations studies is not required, as bifurcations are mainly associate with other components of the system and are not largely affected by the transmission line model.

A methodology is introduced to model the entire power system primarily with differential equations and linear algebraic constraints. The algorithm is proposed to eliminate the possibility of the algebraic equations becoming singular in stability analysis. The generalized form of the proposed model allows for the incorporation of all dynamic load and generator models into the system.

The major contributions of this thesis can then be summarized as follows:

1. A complete bifurcation analysis of different order models in a sample system is presented.

2. Minimum dynamic models which capture the most relevant dynamic characteristics needed for bifurcation analysis are determined.

3. Dynamic models for transmission lines including shunt capacitance and ULTC transformers are proposed.

4. A methodology to implement these models into stability analysis is presented.

5. A power system model that removes nonlinear algebraic constraints is proposed and tested.

The next step in this research is to test the proposed system model in larger systems. By comparing the minimum dynamic models required to

detect bifurcations in several systems, more generalized guidelines could be made as to which detail of modeling is appropriate. Considering larger systems will require the development and use of more robust computational tools to handle the large number of differential equations.

Appendix A

List of Principal Symbols

λ	-	bifurcation parameter
μ	-	eigenvalue
T_0	-	limit cycle initial period
β	-	magnitude of imaginary component of an eigenvalue
M_λ	-	monodromy matrix
K_r	-	generalized reference frame transformation matrix
L_s	-	leakage inductance
L_m	-	magnetizing inductance
L_{load}	-	inductive load inductance
L_{ln}	-	transmission line inductance
$i_a\ i_b\ i_c$	-	instantaneous stator phase current
$i_A\ i_B\ i_C$	-	instantaneous rotor phase current
i_{qs}	-	instantaneous stator q-axis current
i_{ds}	-	instantaneous stator d-axis current
i_{qr}	-	instantaneous rotor q-axis current
i_{dr}	-	instantaneous rotor d-axis current
i_{load_q}	-	instantaneous inductive load q-axis current
i_{load_d}	-	instantaneous inductive load d-axis current
v_qs	-	instantaneous machine stator q-axis voltage
v_ds	-	instantaneous machine stator d-axis voltage
v_{fd}	-	instantaneous synchronous machine field voltage
v_q	-	instantaneous bus q-axis voltage
v_d	-	instantaneous bus d-axis voltage

V_t	-	instantaneous bus voltage magnitude
s	-	induction motor slip
$\psi_a\ \psi_b\ \psi_c$	-	instantaneous stator flux linkage
$\psi_A\ \psi_B\ \psi_C$	-	instantaneous rotor flux linkage
ψ_{qs}	-	instantaneous stator q-axis flux linkage
ψ_{ds}	-	instantaneous stator d-axis flux linkage
ψ_{qr}	-	instantaneous rotor q-axis flux linkage
ψ_{dr}	-	instantaneous rotor d-axis flux linkage
H	-	machine inertia
ω_r	-	instantaneous rotor angular speed
ω_e	-	base synchronous speed
ω_b	-	reference frame speed
X_{ls}	-	stator leakage impedance
X_{lr}	-	rotor leakage impedance
X_m	-	machine mutual impedance
X_{th}	-	synchronous generator Thevenin impedance
r_s	-	machine stator resistance
r_r	-	machine rotor resistance
p_s	-	instantaneous machine stator power
T_e	-	instantaneous machine electrical torque
T_m	-	instantaneous machine mechanical torque
X_q	-	synchronous machine stator q-axis reactance
X_d	-	synchronous machine stator d-axis reactance
ψ_{kq1}	-	synchronous machine q-axis primary damper winding flux linkage
ψ_{kq2}	-	synchronous machine q-axis secondary damper winding flux linkage
T_t	-	ULTC Transformer time constant
a	-	ULTC Transformer secondary tap shift

Bibliography

[1] R. Seydel, *From Equilibrium to Chaos—Practical Bifurcation and Stability Analysis*. Elsevier Science, North-Holland, 1988.

[2] T. Y. J. Lem and R. T. H. Alden, "Comparison of experimental and aggregated induction motor responses," IEEE/PES 94 WM 168-5 PWRS, New York, NY, January 1994.

[3] L. H. Fink, editor, *Proc. Bulk Power System Voltage Phenomena II—Voltage Stability and Security*, ECC Inc., Fairfax, VA, August 1991.

[4] L. H. Fink, editor, *Proc. Bulk Power System Voltage Phenomena—Voltage Stability and Security*, EL-6183, EPRI, January 1989.

[5] L. H. Fink, editor, *Proc. Bulk Power System Voltage Phenomena III—Voltage Stability and Security*, ECC Inc., Fairfax, VA, August 1994.

[6] V. Ajjarapu and B. Lee, "Bifurcation theory and its application to nonlinear dynamical phenomena in an electrical power system," *IEEE Trans. Power Systems*, vol. 7, no. 2, February 1992, pp. 424–431.

[7] C. A. Cañizares, "On bifurcations, voltage collapse and load modeling," *IEEE Trans. Power Systems*, vol. 10, no. 1, February 1995, pp. 512–522.

[8] H. D. Chiang, C. W. Liu, P. P. Varaiya, F. F. Wu, and M. G. Lauby, "Chaos in a simple power system," *IEEE Trans. Power Systems*, vol. 8, no. 4, November 1993, pp. 1407–1417.

[9] C. A. Cañizares and William D. Rosehart, "Bifurcation analysis of induction motor loads for voltage collapse studies," *Proc. NAPS*, M.I.T. Cambridge, Massachusetts, November 1996, pp. 559–565.

[10] B. C. Lesieutre, P. W. Sauer, and M. A. Pai, "Transient algebraic circuits for power system dynamic modelling," *Electrical power and Energy Systems*, October 1993, pp. 315–321.

[11] D.H. Popovic, I.A. Hiskens, and D. J. Hill, "Stability analysis of induction motor networks," technical report, Technical Report, University of Sydney, Sydney, NSW 2006, Australia.

[12] N. U. Krantz M. N. Gustafsson and J. E. Daalder, "Voltage stability: the significance of induction motor loads," *Proc. NAPS*, Bozeman, Montana, October 1995, pp. 394–402.

[13] Y.V. Makarov D.H. Popovic, I.A. Hiskens and D. J. Hill, "Tap locking strategies for emergency voltage control in power supply systems," *Proceedings of the 12th Power Systems Computation Conference, Dresden Germany*, vol. 1, August 1996, pp. 309–315.

[14] Y.V. Makarov D.H. Popovic, I.A. Hiskens and D. J. Hill, "Investigation of load-tap changer iteraction," *Electrical Power and Energy Systems*, vol. 18, no. 2, 1996, pp. 81–97.

[15] M. A. Pai, P. W. Sauer, and B. C. Lesieutre, "Static and dynamic nonlinear loads and structural stability in power systems," *Proceedings of the IEEE*, November 1995, pp. 1562–1572.

[16] W. Xu and Y. Mansour, "Voltage stability analysis using generic dynamic load models," *IEEE Trans. Power Systems*, vol. 9, no. 1, 1994, pp. 479–493.

[17] D. J. Hill, "Nonlinear dynamic load models with recovery for voltage stability studies," *IEEE Trans. Power Systems*, vol. 8, no. 1, February 1993, pp. 166–176.

[18] D. Karlsson and D. J. Hill, "Modelling and identification of nonlinear dynamic loads in power systems," *IEEE Trans. Power Systems*, vol. 9, no. 1, February 1994, pp. 157–166.

[19] M. M. Begovic and R. Q. Mills, "Load identification and voltage stability monitoring," IEEE/PES 94 WM 213-9 PWRS, New York, NY, January 1994.

[20] P. W. Sauer B. C. Lesieutre and M. A. Pai, "Development and comparative study of induction machine based dynamic P, Q load models," IEEE/PES 94 WM 166-9 PWRS, New York, NY, January 1994.

[21] C. A. Cañizares and S. Hranilovic, "Transcritical and Hopf bifurcations in ac/dc systems," pp. 105–114 in [5].

[22] C. A. Cañizares, "Conditions for saddle-node bifurcations in ac/dc power systems," *Int. J. of Electric Power & Energy Systems*, vol. 17, no. 1, February 1995, pp. 61–68.

[23] C. A. Cañizares, F. L. Alvarado, C. L. DeMarco, I. Dobson, and W. F. Long, "Point of collapse methods applied to ac/dc power systems," *IEEE Trans. Power Systems*, vol. 7, no. 2, May 1992, pp. 673–683.

[24] F. L. Alvarado and T. H. Jung, "Direct detection of voltage collapse conditions," pp. 5.23–5.38 in [4].

[25] C. A. Cañizares and F. L. Alvarado, "Point of collapse and continuation methods for large ac/dc systems," *IEEE Trans. Power Systems*, vol. 8, no. 1, February 1993, pp. 1–8.

[26] V. Ajjarapu and C Christy, "The continuation power flow: A tool for steady state voltage stability analysis," *IEEE Trans. Power Systems*, vol. 7, no. 1, February 1992, pp. 416–423.

[27] H. D. Chiang, A. J. Flueck, K. S. Shah, and N. Balu, "CPFLOW: A practical tool for tracing power system steady-state stationary behavior due to load and generation variations," *IEEE Trans. Power Systems*, vol. 10, no. 2, May 1995, pp. 623–634.

[28] The Math Works Inc., Natick, Massachusetts, *MATLAB*, 1993.

[29] E. Doedel X. Wang A. Champneys T. Fairgrieve B. Sandstede Y. Kuznetsov and T. Fairgrieve, "Auto97 continuation and bifurcation software for ordinay differential equations," technical report, California Institute of Technology, Pasadena, CA 91125, 1997.

[30] C. A. Cañizares, A. Z. de Sousa, and V. H. Quintana, "Improving continuation methods for tracing bifurcation diagrams in power systems," pp. 349–358 in [5].

[31] John H. Mathews, *Numerical Methods for Mathematics, Science, and Engineering, Second Edition.* Prentice Hall, Englewood Cliffs, New Jersey, 1992.

[32] R. H. Park, "Two-reaction theory of synchronous machines-generalized methods of analysis-part 1," *AIEE Trans.*, vol. 48, July 1929, pp. 716–727.

[33] P. C. Krause, O. Wasynczuz, and S. D. Sudhoff, *Analysis of Electric Machinery.* IEEE Press, New York, 1995.

[34] Prabha Kundur, *Power Systen Stability and Control.* McGraw Hill Publishing Company, New York, 1994.

[35] Paul L. Cohran, *Polyphase Induction Motors: Analysis, design and application.* Marcel Dekker, Inc, New York, 1989.

[36] Edward L. Owen, "Evolution of induction motors - the ever-shrinking motor," *IEEE Industry Applications Magazine*, vol. 3, no. 1, 1997, pp. 16–18.

[37] Stephen J. Chapman, *Electric Machinery Fundamentals.* McGraw Hill Publishing Company, New York, 1991.

[38] Anderson and Fouad, *Power System Control and Stability.* The Iowa State University Press, Ames Iowa, 1977.

[39] P. W. Sauer and M. A. Pai, "A comparison of discrete vs continuous dynamic models of tap-changing-under-load transformers," *Proc. NSF/ECCC Workshop on Bulk Power System Voltage Phenoma III: Voltage Stability, Security and Control, Davos, Switzerland,* August 1994.

[40] J. DiManno, G. J. Rogers, and R. T. H. Alden, "An aggregated induction motor model for industrial plants," *IEEE Trans. Power Apparatus and Systems*, vol. 103, no. 4, April 1984, pp. 683–690.

[41] V. Venkatasubramanian, H. Schättler, and J. Zaborszky, "A taxonomy of the dynamics of the large power systems with emphasis on its voltage stability," pp. 9–52 in [3].

[42] B. W. Char et al, *Maple V Language Reference Manual*. Springer-Verlag, 1991.

[43] F.L. Alvarado, *Electromagnetic Transient Program Volume 3: Workbook III*. Electric Power Research Institute, Palo Alto, California, 1989.